Journal of Renewable Materials

Tech Science Press

https://doi.org/10.32604/jrm.2026.02025-0233

REVIEW

Spotlight on Sustainable Biobased Carbon Catalysts: Recent Progress and Cross-Cutting Opportunities in Catalysis, Photochemistry and Electrochemistry

Kelly Leite dos Santos Castro Assis[1], Druval Santos de Sá[1], Bruno da Silva Marques[1], Carolina Carvalho de Mello[1], João Lucas Marques Barros[2], Henrique Carvalhais Milanezi[2], João Batista Oliveira dos Santos[2], Carlos Alberto Franchini[1], Bráulio Soares Archanjo[1], Carlos Alberto Achete[1] and Adriana Maria da Silva[1,*]

[1]Divisão de Materiais, Instituto Nacional de Metrologia, Qualidade e Tecnologia (INMETRO), Duque de Caxias, RJ, Brazil
[2]Departamento de Engenharia Química, Universidade Federal de São Carlos (UFSCAR), São Carlos, SP, Brazil

*Corresponding Author: Adriana Maria da Silva. Email: amdasilva@inmetro.gov.br

Received: 31 December 2025; Accepted: 30 April 2026; Published: 28 July 2026

ABSTRACT: The transition toward a circular economy and zero-waste strategies has driven increasing interest in biomass-derived carbon materials as sustainable alternatives to conventional catalyst supports. Agricultural and industrial residues can be converted into porous carbons with high surface area, tunable porosity, and rich surface chemistry, enabling waste valorization and stabilization of metal species ranging from nanoparticles to single atoms. These properties support their application across heterogeneous catalysis, photocatalysis, and electrochemical systems, revealing cross-cutting opportunities among these fields. Despite these advantages, challenges remain, including feedstock heterogeneity, energy-intensive processing, scalability limitations, and the lack of standardized methodologies. This review highlights recent advances in the development of sustainable carbon catalysts, focusing on shared limitations and the relationships between structure, properties, and applications. In addition, it discusses key factors influencing material performance and long-term viability. Emphasis is placed on future perspectives that align with circular economy principles and low-waste strategies, aiming to guide the design of more efficient, scalable, and environmentally responsible catalytic systems.

KEYWORDS: Biomass-derived carbon materials; sustainable catalysis; functional carbon materials

1 Introduction

The requirement for a zero-waste process triggered the search for new raw materials and a process with a zero-waste approach aligned with the expression "from cradle to cradle," encompassing reusing, recycling, and recovering. The design of the entire process must ensure minimal generation of by-products and energy consumption. In this scenario, alternative processes and resources have been considered, such as the utilization of CO_2, CH_4 (from landfills, biodigesters or biomass gasification); used cooking oil; biomass from agriculture or plastic recycling. All these feedstocks can serve as promising primary materials for the synthesis of chemicals, fuels, and porous materials for heterogeneous catalysts, photocatalysts, and electrochemical materials. Biomass derivatives stand out as a potential source for the synthesis of numerous materials for a broad range of applications, aiding in biomass waste management. Biomass is abundant in agricultural countries such as Brazil, India, China, Thailand, and Colombia, which are uniquely positioned to leverage this technology by converting low-cost agricultural residues into high-value carbon materials [1]. In Brazil, the world's leading sugarcane producer, materials like sugarcane bagasse and coffee husks offer

tremendous potential [2]. Similarly, India's rice husks [3], China's corn stover [4], Thailand's coconut shells [5] and Colombia's palm oil residues [6] represent valuable feedstocks for producing carbon-based materials [7]. However, agricultural residues present significant challenges for disposal. Utilizing biomass offers an opportunity to produce value-added products sustainably, while minimizing waste generation and aligning with circular economy principles [1].

One potential application relies on the development of porous materials from biomass-derived carbon, with application in sustainable processes in distinct areas such as heterogeneous catalysis, photocatalysis, and electrochemistry, including electrocatalysis, due to the shared properties critical for these fields. These applications require high porosity, high specific surface area, and abundant anchoring sites to enhance catalytic stability, charge transfer, and stabilization of metallic particles in heterogeneous catalysts. Sustainable materials, such as those derived from biomass, offer tunable properties, cost-effectiveness, and environmental benefits, making them ideal candidates for advancing these technologies [8,9].

The synthesis of sustainable carbonaceous materials can utilize a wide range of biomass, which can be categorized based on their sources: agricultural residues (e.g., rice husks, corncobs, wheat straw, fruit stones), forestry byproducts (e.g., wood, bamboo, palm and kernel shells), animal-derived wastes (e.g., eggshells, mollusk shells), industrial byproducts (e.g., weak black liquor from pulp and paper processing), and other waste materials (e.g., plastic waste). Additionally, CH_4 derived from landfill biogas can serve as an indirect carbon source for energy-intensive synthesis processes or as a precursor for carbon-based materials. The choice of biomass is heavily influenced by regional availability, which varies across countries and enables localized, cost-effective sourcing. This diversity reduces reliance on non-renewable feedstocks and minimizes transportation-related costs and emissions [9,10].

Nevertheless, a potential challenge lies in the variability of biomass characteristics. Vegetal biomass, for example, depends on distinct factors such as the type of plant and soil conditions. This inherent variability directly influences the structural and chemical properties of the derived carbonaceous materials. Biomass composition can change considerably in terms of cellulose, hemicellulose, lignin, organic and inorganic compounds, which might drastically affect the final properties of the catalysts. The use of biomass without extensive purification can be advantageous in terms of sustainability and cost; however, pre-treatment or purification becomes necessary when inorganic contaminants significantly influence carbon structure, active-site formation, or catalytic performance. In particular, lignocellulosic biomass, such as coconut shells or bamboo, typically contains high levels of lignin and cellulose, which contribute to a high carbon (C) yield and structural stability during carbonization or activation processes [11]. In contrast, animal-derived wastes like eggshells are rich in calcium carbonate, requiring additional processing to produce porous carbon structures. The chemical composition (e.g., lignin, cellulose, hemicellulose, or ash content) and physical properties (e.g., density and particle size) of the biomass influence key parameters of the final material, such as surface area, pore size distribution, and surface chemistry. Typical inorganic contaminants, such as Na, K, P, Fe, Mg, and Si, must be considered. For example, rice husks, with their high Si content, can yield carbonaceous materials with unique textural properties suitable for specific adsorption applications. In this context, the use of biomass without further purification to remove inorganic contaminants should be prioritized in order to fulfill environmental and economic requirements. Moreover, this versatility in the selection of biomass sources aligns with the evolving global energy landscape, which increasingly emphasizes region-specific renewable resources to promote sustainability and mitigate environmental impacts. By utilizing locally abundant biomass, the production of carbonaceous materials adheres to sustainability, converting waste streams into valuable products such as porous carbon for distinct applications such as heterogeneous, photocatalysts and electrodes.

Despite their potential, several hurdles need to be addressed to enable the safe and economically competitive compared to conventional raw materials. Furthermore, biomass processing is energy-intensive,

reflecting in the final costs. The lack of standardized procedures, coupled to inadequate purification methodologies remains a significant obstacle to overcome, impacting negatively the final costs of the material [12–14]. Furthermore, in this overview, the term "biomass-derived carbon materials" is used to collectively describe carbon materials obtained from renewable biomass sources, including metal-free carbons, heteroatom-doped carbons, and carbon-supported single-atom catalysts, unless otherwise specified.

Accordingly, this review is structured into three primary sections addressing the applications of biomass-derived carbons in catalysis, photocatalysis, and electrochemistry, alongside broader considerations including economic viability and future prospects. However, the objective of this work is not to provide a comprehensive survey of sustainable carbon materials for these applications, given the existence of several authoritative reviews on the subject [1,8–10,13,15]. Instead, it focuses on representative and conceptually relevant advances reported primarily over the past decade, selected to highlight key design principles, challenges, and cross-cutting trends in biomass-derived carbon catalysts. Unlike existing reviews that primarily address biomass-derived carbon materials within individual application domains, this work adopts a cross-cutting perspective by comparatively analyzing heterogeneous catalysis, photocatalysis, and electrochemistry, with emphasis on shared structure–property–application relationships, transferable design descriptors, and common performance-limiting factors across these fields.

2 Applications in Heterogeneous Catalysis, Photocatalysis and Electrochemistry

2.1 Sustainable Carbon-Based Materials for Heterogeneous Applications

Heterogeneous catalysts play a critical role in industry with over 90% of petrochemical, chemical and food manufacturing processes utilizing heterogeneous catalysts in at least one conversion step. These catalysts typically comprise a small amount of noble or transition metal supported on high-surface-area materials, such as carbon, Al_2O_3, SiO_2, among others. The metal particles are engineered to remain at the nanoscale, smaller than 10 nm, with a narrow size distribution at the support surface. The particles exposed to the reaction at the surface are termed metallic dispersion. Nevertheless, controlling the nanoparticles distribution is still challenging due to their high surface energy, which drives the agglomeration to achieve a lower energy state. To counter this, high surface area support is used to stabilize the nanoparticles and facilitate mass transfer, a key factor since heterogeneous catalysis processes are mass-transfer driven. Currently, distinct methods have been suggested to maintain particles at the nanoscale, including the single-atom scale. Carbon-based materials, such as activated carbon (AC) [16,17], reduced graphene oxide (rGO) [18–22], carbon nitride (g-C_3N_4) [23] carbon nanotubes (CNTs) [24–27], carbon spheres (CS) [28,29], and biochar [30,31], have been explored for their exceptional capacity to promote high metallic dispersion. Hierarchical carbon materials such as AC, rGO, CNT, are particularly valued for their intrinsic attributes, including large specific surface area (often exceeding 500–3000 m^2/g in optimized forms), oxygen vacancies, heteroatoms (N, S), robust thermal and chemical stability, high thermal conductivity, hydrophobicity, and the presence of functional oxygen groups and heteroatoms (e.g., N or S), which serve as interaction centers for stabilizing metal particles. Remarkably, all referenced catalyst supports can be derived from sustainable sources such as vegetal and animal biomass, as well as plastic waste. Additionally, gases generated from biomass conversion, such as methane (CH_4), can serve as precursors for synthesizing carbon supports like CNTs. These carbon-derived materials can be engineered to exhibit hierarchical structures and high specific surface areas, enhancing their utility in catalytic applications.

The field of carbon materials has advanced significantly, with the development of distinct materials derived from different sources of biomass. Among them, the development of metal-free carbon catalysts and single-atom catalysts stands out as potential systems for several catalytic applications [32,33].

2.2 Biomass Derived-Catalysts

Among the biomass derived-catalysts, metal-free carbon catalysts have demonstrated excellent performance in various reactions, as illustrated in Fig. 1. These include alcohol dehydration and dehydrogenation, SO_x and H_2S oxidation, and NO_x reduction. Metal-free carbon catalysts constitute a sustainable alternative [34,35], considering their advantages such as low cost, high activity, stability, and excellent physical and chemical properties [36,37]. Nevertheless, pristine carbon materials are inert and exhibit limited interaction with reactants [38], necessitating surface functionalization or the introduction of heteroatoms into the carbon lattice to enhance their reactivity. Thus, in the design of metal-free carbon catalysts, the presence of well-defined active sites is essential to achieve the desired chemical reactivity. These active sites are typically created through surface functional groups, heteroatom doping (e.g., nitrogen (N), boron (B), phosphorus (P), and sulfur (S)), defect engineering, and/or controlled thermal annealing. The heteroatom incorporation in the sp_2-hybridized carbon frameworks results in charge delocalization and electronic changes, with enhanced catalytic performance. Among these heteroatoms, N is more often used as doping due to its similar atomic diameter to C [39]. The superior activity of N-doped carbon is related to electronic effects, considering its higher electronegativity (3.04) than that of C (2.55). When incorporated into the sp_2 carbon lattice (such as graphene or carbon nanotubes—CNTs), the N atoms withdraw electrons from adjacent C atoms. This electron withdrawal enables a charge redistribution across the structure, thereby inducing an electrophilic (electron-deficient) character on the neighboring C atoms. The choice of the heteroatom will rely on the specific reaction and the required activity, selectivity and stability. However, the N-doped carbons are clearly the preferred supports for both metal and metal oxides. N-doping increases the creation of basic sites, offering benefits in several organic transformations such as hydrogenation and dehydrogenation, oxidation and coupling reactions (Fig. 1) [32].

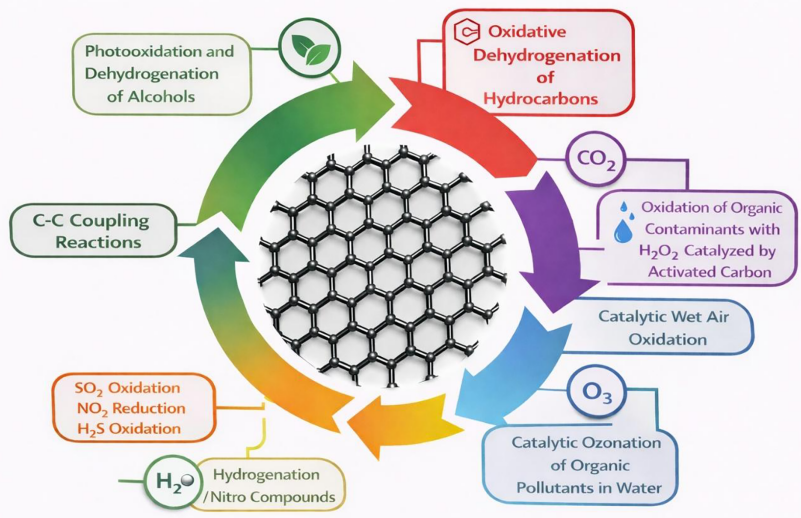

Figure 1: Reactions promoted by N-doped carbons. Adapted from ref. [32]. Copyright 2023 American Chemical Society.

Furthermore, the presence of N atoms into the carbon lattice improves the hydrophilicity due to the introduction of polar groups, altering the electronic distribution, enabling the interaction with other polar groups.

Typically, there are four types of N atoms doping in carbon skeleton which are graphitic N, pyridinic N, pyrrolic N, and pyridinic N-oxide (Fig. 2) [40].

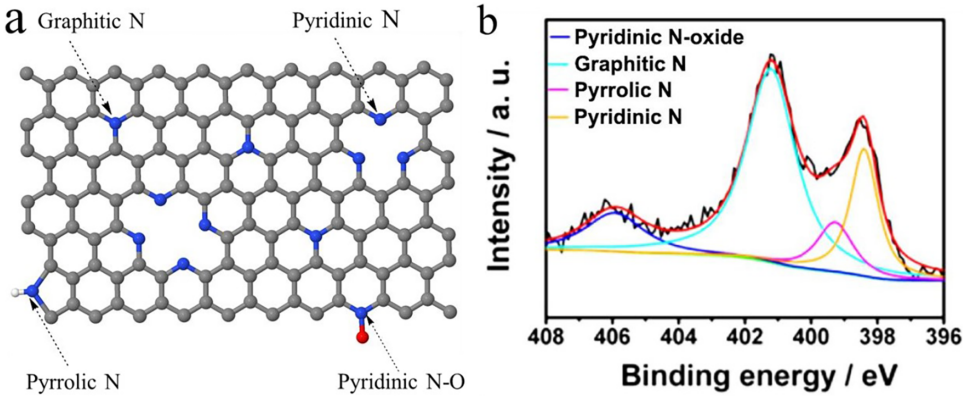

Figure 2: (**a**) Bonding configurations of nitrogen atoms in carbon networks. Reprinted with permission from ref. [40]. Copyright 2017 American Chemical Society and (**b**) XPS spectra of N atoms in different configurations. Reprinted with permission from ref. [40]. Copyright 2014 American Chemical Society.

XPS spectra show clearly these different N groups with the corresponding B. E. for N1s peaks at B. E. of 398.3–399.8, 400.1–400.5, 401.0–401.4, and 404.0–405.6 eV corresponding to nitrogen atoms in the species of pyridinic, pyrrolic, graphitic, and different N-oxide species, respectively. It is known that N in nitrogen-doped carbon materials (N-CNMs) occurs in the graphite-like configuration, where it is integrated into the planar structure by substitution of carbon atoms in the hexagonal graphitic structure [40].

Other Heteroatoms as doping for carbon catalysts: As discussed earlier, nitrogen remains the most extensively utilized heteroatom owing to its favorable electronic and structural properties. However, other heteroatoms, such as S, B, P, and O, are also incorporated, often in co-doping configurations with N to harness synergistic enhancements in catalytic performance. Table 1 presents a comparative overview of the primary properties of these heteroatoms, along with the catalytic reactions they predominantly promote.

Table 1: Heteroatom-doping properties, effects and catalyzed reactions.

Heteroatom	Electronegativity	Atomic Radius (pm)	Predominant Effect	Reactions
C	2.55	77	–	–
N	3.04	71	Creation of electron deficient on neighboring C atoms	Dehydrogenation, oxidation, coupled reactions [38,41]
S	2.58	105	Alteration of spin density and creation of “strain” in the lattice without changing the charge.	Selective oxidation, hydrogenation and redox reactions [38]
P	2.19	98	Introduces significant structural defects and surface oxygen groups due to its large atomic radius.	Alcohol dehydrogenation [38,42], alcohol selective oxidation [43]

(Continued)

Table 1 (continued)

Heteroatom	Electronegativity	Atomic Radius (pm)	Predominant Effect	Reactions
B	2.04	88	Acts as an electron donor to the lattice, creating Lewis acidic sites.	Dehydrogenation and oxidation [38], organic carbonate synthesis [44]

The atomic radius and electronegativity of heteroatoms and C explain their activity in different reactions. The high electronegativity difference between N and C, compared to the other dopants, induces strong charge polarization on adjacent C atoms, creating positively charged active sites. The similar atomic size to C allows the lattice substitution with minimal distortion, enabling high doping levels and structural stability. In contrast, S and P have significantly larger atomic radius than C, affecting the lattice stability. The intermediate size of B induces moderate lattice strain. Nevertheless, B has the lowest electronegativity, which induces electron deficiency (positive on B, negative on the neighboring adjacent C) [38]. The electronegativity of S is nearly identical to that of C, resulting in negligible charge transfer. The role of S contrasts with N doping (charge-dominated), explaining the limited activity of S-doping alone whereas the co-doping with N often results in a synergistic effect, with N providing charge polarization, while S enhances spin density and strain [45]. Regarding P, it has almost the same electronic and chemical properties as C and N; thus, the main contribution arises from the atomic radius difference, creating defective sites, contributing to enhancing the reactivity. A promising approach is the utilization of two or three heteroatoms with different electronegativity, tuning the properties according to the catalytic reaction, resulting in a synergism among the different elements [37].

Metal-free catalysts, co-doped with N and S have demonstrated excellent performance in the hydrodeoxygenation of vanillin, achieving vanillin conversions exceeding 80% and selectivities to 4-methylguaiacol (MMP) of approximately 70% [37]. The authors ascribed this high efficiency to synergistic effects between N and S doping, combined with elevated surface areas and structural defects.

In another study, N-doped carbon materials derived from biomass, namely chitosan, which served as both C and N sources, were prepared using HNO_3 as a solvent and evaluated for the selective oxidation of D-xylose to D-xylonic acid under mild reaction conditions (10 bar O_2, 100°C) [41]. The superior performance obtained on the optimized catalyst was attributed to the abundance of graphitic N moieties. These N-containing species generate medium-strength basic sites, which facilitate activation of the aldehyde group and promote carboxyl group formation during the selective oxidation process.

A catalyst was prepared from spent coconut-based activated carbon (CAC) previously used for the adsorptive removal of neutral red (NR) dye [46]. The material was calcined under an N_2 atmosphere at 800°C, yielding N-doped CAC. The resulting catalysts were evaluated in the hydrochlorination of acetylene, in which the NR-derived catalysts exhibited superior performance compared to undoped CAC, achieving higher acetylene conversion. The activity was correlated with the N content. Density functional theory (DFT) calculations revealed that pyridinic and pyrrolic N-species serve as the primary active sites for the reaction. Additionally, the inherent mesoporosity of the CAC played a crucial role in enhancing overall catalytic performance.

Starch biomass was used for the synthesis of P-doped carbon materials employing H_3PO_4 under different pyrolysis temperatures, yielding multilayered structures. The catalysts were evaluated in the selective

aerobic oxidation of alcohols, with the enhanced performance attributed to the presence of P–O moieties and associated defects. The P–O–C species and the defects generated by P–O doping were identified as the active sites for benzyl alcohol conversion. Furthermore, Raman spectroscopy results revealed a clear correlation between turnover frequency (TOF) and the oxidation reaction activity. Despite the high surface areas obtained for the various samples, no evidence of correlation with catalytic activity was found, indicating that the predominant role arises from the defective structure generated by P–O moieties [43]. The catalysts exhibited sustained stability, retaining their performance even after eight cycles of reuse.

The aforementioned examples demonstrate the feasibility of synthesizing doped metal-free carbon catalysts and their remarkable performance in various relevant processes, along with their potential for recyclability. The sites generated by carbon doping also play a crucial role in the stabilization of metallic nanoparticles, even at the atomic scale, as briefly discussed in the following paragraphs.

In this regard, single-atom catalysts (SACs) have emerged as a sophisticated approach in catalyst design, wherein carbon-based SACs have garnered considerable interest due to their tunable morphologies, well-developed porosity, and rich surface chemistry featuring abundant functional groups. The term single-atom catalysts (SAC) was introduced by the seminal work of Qiao et al. in 2011, which demonstrated the preparation and superior catalytic performance of a Pt single-atom catalyst supported on FeO_x (Pt_1/FeO_x) for CO oxidation. This study effectively established the concept of single-atom catalysis and highlighted its potential as a powerful approach to maximize metal atom utilization by reducing particle size to the atomic limit [47]. SACs also challenge conventional catalyst design by decoupling activity enhancement from metal loading, thereby shifting the focus toward coordination environment control and support chemistry rather than particle size alone.

In heterogeneous catalysis design, stabilizing metal particles at the nanoscale is a critical parameter, as metal particle size profoundly influences performance in numerous reactions. Furthermore, reducing the size of metallic particles confers additional benefits to catalytic behavior, as comprehensively reviewed by Yang et al. in 2013 [48]. These include: (i) the creation of low-coordination environments at metal centers arises from the higher proportion of unsaturated surface atoms in smaller particles; (ii) quantum size effects emerge from the spatiality of electron confinement in nanoscale structures. Resulting in the discretization of energy levels and in a pronounced increase in the energy separation between the highest occupied molecular orbital (HOMO) and the lowest unoccupied molecular orbital (LUMO); (iii) enhanced metal–support interactions at the interface, which facilitate charge transfer between the metal and the support. Collectively, these factors contribute to enhancing the activity, selectivity, and stability in supported metal catalysts. While these effects are well established for metal nanoparticles, their arrangement at the single-atom limit introduces distinct electronic and coordination constraints that fundamentally alter reaction pathways and stability trends.

Regarding SACs production from biomass, heteroatom doping provides anchoring sites for metal immobilization, thereby facilitating the stabilization of metal atoms at the nanoscale, including at the single-atom level. This approach is of fundamental importance, considering that the activity and yields of many relevant industrial processes still depend on transition or noble metals. The use of doped carbon as a support not only strengthens the metal–support interaction but also provides sites that enhance metal dispersion and introduce acid–base functionalities [49]. Additionally, it enables straightforward metal recovery through combustion of the carbon skeleton. However, the effectiveness of heteroatom doping strongly depends on dopant type, concentration, and spatial distribution, which remain difficult to control in biomass-derived carbons. This variability introduces trade-offs between catalyst performance, synthesis reproducibility, and scalability that are often underexplored in laboratory-scale studies, highlighting the need for more systematic evaluation in future research.

These considerations highlight that, despite their promising activity, the practical deployment of biomass-derived SACs requires balancing atomic dispersion, long-term stability, and sustainable synthesis routes.

Carbon-derived SACs have been applied in numerous heterogeneous catalyzed reactions in addition to photocatalysis and electrocatalysis [50], as shown in Fig. 3.

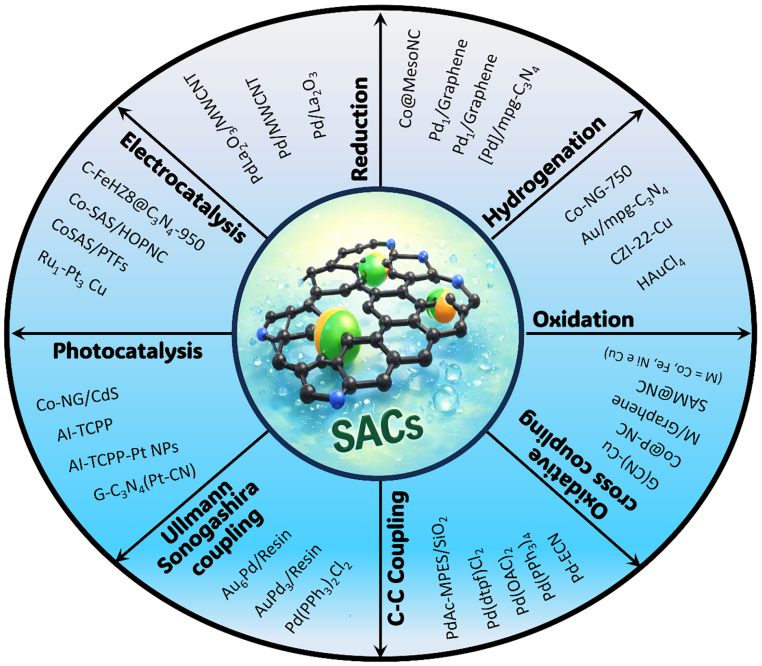

Figure 3: Applications of carbon-based SACs. Adapted from [51]. Copyright 2020 American Chemical Society.

SACs derived from a variety of biomass sources have been detailed [51]. Biomass is rich in nitrogen and oxygen functional groups, serving as self-doping for the single atom during pyrolysis at high temperature, producing N-doped biochar, without the need for toxic reactants to make the synthesis greener [49,51]. The interest in biomass-derived carbon as support for SACs dates to 2018 [52–55].

Derived lignin SACs, Co/Mn and Co supported on N-doped SA were evaluated in the aerobic oxidation of 5-hydroxymethylfurfural (HMF) to 2,5-furandicarboxylic acid (FDE) [56]. The excellent activity was correlated with the tuning of the electronic structure of metallic nanoparticles (NPs) embedded in the lignin structure. Similarly, lignin was used as a strategy for confining metal ions within a metal-lignin complex. DFT theoretical calculations demonstrated that Co-N_3C sites were the centers responsible for the conversion of HMF to 2,5-furandicarboxilato de dimetila (FDME) [57]. Also, the authors highlight that the atomically dispersed Co active sites (Co–N_x) are responsible for the high efficiency and selectivity in the simultaneous oxidation of the alcohol and aldehyde groups of HMF into ester groups. Both investigations demonstrated the recyclability of the SACs without loss of integrity.

Recently, chitin-derived supramolecular nanowires-stabilized single-atom Pt catalysts (SS-Pt-CSNs) were evaluated in the selective hydrogenation of 31 α,β-unsaturated compounds (C=C, C=O, C≡C, –NO_2) including nitroarenes and unsaturated aldehydes with excellent chemoselectivity. The stability of the catalyst was confirmed by recycling experiments without affecting its stability. DFT was used for determining the four coordination models and the supramolecular structure of chitin from XAS results. EXAFS results revealed three O/N atoms surrounding a Pt single atom, and also four O/N atoms were considered in the model.

Apart from the mentioned catalytic systems, numerous biomass-derived catalysts have been prepared and tested in heterogeneous catalytic reactions, and some examples are presented below.

Orange peel industrial waste was used for producing a carbon support for Pt (0.5%, wt) and used in the guaiacol hydrodeoxygenation, activated with H_3PO_4, leading to the formation of P–O species on the support. The presence of P-O moieties favored the formation of highly dispersed and active Pt nanoparticles, with concomitant superior catalytic performance. The enhanced catalytic activity and selectivity were attributed to the increased surface acidity induced by H_3PO_4 activation, which acts as a promoter through the incorporation of phosphorus-containing species. The outstanding performance of the optimized catalyst Pt-ACS was explained by a strong synergistic effect between the acidic sites provided by the phosphorylated support and the metallic Pt sites during the hydrodeoxygenation (HDO) of guaiacol.

Olive stone was used as a carbon source for the synthesis of a catalyst (CB), which was subsequently evaluated in the methoxylation of α-pinene at atmospheric pressure (1 atm) and temperatures ranging from 50°C to 65°C. The performance of this catalyst was compared with that of a carbon xerogel (CM) and a commercial activated carbon from Norit (NoritN) [58]. The CB exhibited catalytic behavior similar to the reference materials. Despite some textural differences among catalysts, the key factor governing the catalytic behavior was associated with the surface acidity. Both the strength and accessibility of the acid sites played a crucial role in the good performance of CB. Nevertheless, severe deactivation was observed after the second reaction cycle, although selectivity was maintained. Analysis of the spent catalyst by XPS revealed that some surface functional groups were likely modified, probably due to esterification of carboxylic acid groups caused by the excess methanol in the reaction medium.

Activated carbons (AC) were produced from the woody part of tea, which is highly available after the harvesting of tea leaves through activation and carbonization treatments. The AC produced was used as a support for Co, Ni and Cu nanoparticles and used in the H_2 production from NH_3BH_3. The results reveal that Co nanoparticles with an average particle size of 3.18 nm on the AC support showed superior performance compared to Cu and Ni. Recyclability of the catalysts was evaluated over 5 cycles, with a loss of 40% after the second cycle [59].

Char-derived biomass residues were collected from a Tyrol gasifier plant (Italy) and used to prepare Co- and Fe-based catalysts (10 wt%) for evaluation in the Fischer-Tropsch (FT) reaction [60]. Compared with Fe, Co deactivated rapidly due to its susceptibility to chemical poisoning by inorganic contaminants (K, Mg, S). Furthermore, the authors observed an unexpected increase in SSA upon metal incorporation, which was attributed to the synthesis methodology. Additionally, TEM results indicated that the Fe particle size was below 4 nm whereas Co particles were significantly higher, with a bimodal distribution, ranging from 8–11 nm.

Aside from the previous discussion, it is noteworthy that CNTs can also be synthesized from biomass precursors through processes such as pyrolysis or chemical vapor deposition, or even from CH_4 derived from pyrolysis or even from landfill gases. Biomass-derived CNTs are formed through carbon decomposition followed by structural rearrangement into nanotubes. The growth of CNTs can be enhanced by catalysts or minerals naturally present in the biomass. Carbon materials synthesized by microwave-assisted methods are an interesting approach because higher temperature homogeneity can be obtained by using microwave [61]. In addition, more energy effective heating in less time can be reached using a microwave compared to conventional heat sources.

The efficiency of CNTs has been proven in several heterogeneous catalytic reactions such as steam reforming (ethanol, glycerol), CO_2 hydrogenation [27,62,63]. CNTs often yield structures with high conductivity, mechanical strength, and excellent performance as supports or metal-free catalysts in heterogeneous

catalysis applications. The metal confinement effect provided by CNTs results in systems with nanosized metallic catalysts [27]. Notably, beyond porous carbons, biomass-derived carbon nanotubes represent another promising class of materials obtainable via sustainable routes, exhibiting superior electrical conductivity and serving as effective supports for metal nanoparticles in heterogeneous catalysis.

Overall, despite the high potential of biomass-derived supports, some aspects remain challenging, specifically related to the limits of metal loading. Regarding biomass-derived supports, it is accurate that conventional SACs on such materials frequently exhibit metal loadings below 1 w.t% (and often in the range of 0.5–1.5 wt.%) to preserve atomic dispersion. This limitation arises primarily from the inherent high surface energy of isolated metal atoms, which promotes aggregation into clusters or nanoparticles during synthesis (e.g., pyrolysis) or under operational conditions. Biomass-derived carbons, while sustainable and rich in heteroatoms (N, O, S) that facilitate coordination, typically provide moderate-to-weak metal-support interactions compared to engineered supports like MOF-derived or defect-rich materials. Consequently, insufficient anchoring sites or suboptimal pore structures can lead to migration and sintering, compromising long-term stability.

A critical trade-off exists between increasing metal loading density to enhance the number of active sites (and thus overall catalytic performance per unit mass) and maintaining atomic isolation to avoid aggregation. Higher loadings (HL) amplify site density and may introduce beneficial inter-site synergies or modified electronic effects; however, they shorten inter-atom distances, heightening the risk of Ostwald ripening, thermal migration, or leaching, particularly in demanding reaction environments. Recent advances have mitigated this through strategies like multilayer stabilization, defect engineering, or precursor design (e.g., urea-assisted coordination or sulfide-mediated atom trapping), enabling loadings up to 5–10 wt.% or higher in select cases without loss of single-atom character [64]. Nonetheless, achieving elevated loadings while ensuring robust stability remains challenging and often requires tailored heteroatom doping or hierarchical structuring.

Although the sustainability appeal of biomass-derived carbon materials is attractive, their synthesis often involves energy-intensive steps such as high-temperature pyrolysis, chemical activation, and heteroatom doping, which increase the overall environmental footprint. Future efforts should therefore focus on lower-temperature processes, milder activation methods, and the use of biomass-inherent heteroatoms to balance catalytic performance with sustainability and enable scalable, low-energy synthesis routes. Nevertheless, detailed life-cycle assessment and techno-economic analyses remain scarce for many biomass-derived carbon systems, available studies consistently indicate that feedstock availability, energy consumption during synthesis, and process scalability are key factors governing their environmental and economic viability.

2.3 Sustainable Carbon-Based Materials for Photocatalytic Applications

The development of sustainable carbon-based photocatalysts derived from biomass has emerged as a crucial strategy for addressing environmental and energy challenges worldwide [65–68]. The advantages of biomass-derived photocatalysts are manifold: their hierarchical porous structure, oxygen-rich surface chemistry, and excellent charge transport properties enhance photocatalytic efficiency for applications ranging from water purification to renewable hydrogen production [69–72]. These recent studies have highlighted the remarkable potential of biomass-derived materials as photocatalysts for environmental remediation and renewable energy production. Biomass-based carbon materials, as reviewed by Wang et al. (2021), exhibit high porosity and oxygen-rich surface functionalities such as hydroxyl and carboxyl groups, which enhance pollutant adsorption and provide abundant active sites for photocatalytic reactions. Furthermore, their excellent electrical conductivity facilitates efficient charge separation and transfer, significantly improving the degradation efficiency of organic contaminants under visible light [73]. Biochar, produced

via controlled biomass pyrolysis, has emerged as a promising photocatalyst support owing to its porous structure and high density of oxygenated functional groups. These features enhance both adsorption capacity and interfacial charge transfer. Moreover, biochar acts as an effective electron reservoir, reducing electron-hole recombination and extending light absorption into the visible range by narrowing the band gap of the semiconductor [71]. A study demonstrated the successful fabrication of hierarchical porous TiO_2 structures using wood as a natural template. By integrating CdS and noble metals to form ternary heterojunctions, the resulting photocatalyst exhibited improved mass transport, efficient light harvesting, and enhanced charge carrier separation. Notably, the photocatalytic hydrogen evolution rate increased by up to 6.7 times compared to non-templated systems, demonstrating the key role of hierarchical porosity and interface engineering [70].

The valorization of lignocellulosic biomass for environmental applications has been widely reported. The intrinsic three-dimensional porous architecture of lignocellulosic materials, combined with their oxygen-rich surface chemistry, promotes high adsorption capacity and enhances the photocatalytic degradation of pollutants in both aqueous and gaseous media. In addition, surface functional groups facilitate stronger interactions between the photocatalyst and target contaminants while improving charge carrier dynamics [69]. Finally, a 2021 review focused on biochar-based nanocomposites for the photocatalytic degradation of emerging organic pollutants highlighted the synergistic effects of biochar's large surface area, high porosity, and oxygen-rich surface functionalities in enhancing pollutant adsorption and promoting the generation of reactive species [74]. The authors highlighted the synergistic effects of biochar's large surface area, high porosity, and oxygen-rich surface functionalities in improving pollutant adsorption and enhancing reactive species generation. Additionally, the presence of biochar reduces electron-hole recombination and significantly improves visible-light-driven photocatalytic performance. Overall, these studies underscore that the hierarchical porous structure, oxygen-rich surface chemistry, and superior charge transport properties inherent to biomass-derived photocatalysts play a pivotal role in enhancing photocatalytic efficiency for a broad range of applications, from water purification to renewable hydrogen production.

Among the various materials that can be obtained from biomass, g-C_3N_4 appears as a potential carbon-derivative with potential applications in distinct areas. The polymeric carbon nitride allotrope g-C_3N_4 is a melamine-like molecular framework, based on triazine or tri-s-triazine monomer rings (Fig. 4), organized on defective microstructured lamellar nanosheets whose basal planes possess interplanar distances of around 3 Å and lateral dimensions on the micrometric scale, ensuring large surface areas, consequently enhancing its field of application. It is regarded as one of the oldest synthetic polymers, produced by Berzelius and named by Liebig as "melon" in 1834. More than 180 years after this discovery, dozens of synthetic methodologies have been widely developed, and numerous purposes are now known [75,76].

When compared to graphene, wherein covalent C–N bonds form and enhance chemical resistance to water, acids, bases and solvents like ethanol, toluene and THF (or common organic solvents), van der Waals interactions between sheets promote facile exfoliation due to weak interlayer forces [77]. Defects and structural discontinuities in g-C_3N_4 drive its reactivity, enabling its use as a photocatalysts or as anchoring sites for SACs, providing a myriad of possibilities, resulting in highly versatile structures [78].

Since Wang and coworkers revisited g-C_3N_4 and discovered that polymeric carbon nitride exhibits semiconducting behavior and promising photocatalytic performance for hydrogen production from water under solar irradiation, graphitic carbon nitride stands out as one of the most promising non-metallic photocatalysts. The absence of d^0 transition metals or d^{10} post-transition metals, as commonly found in classical photocatalysts, highlights the simplicity and feasibility of this material [79].

The triazinic/heptazinic molecular structure reflects the synthetic approaches employed to build it and is based chiefly on the chemistry of thermal polycondensation of urea [80], thiourea [81], dicyandiamide [82] and melamine, which is also commonly used as a precursor [83]. Although thermal condensation is the main

methodology and solid-state reactions are also reported [76]. Furthermore, several reactants can be used and different intermediates may be involved during the synthesis process of g-C_3N_4. Fig. 5 depicts the main reactants and intermediates involved in the synthesis.

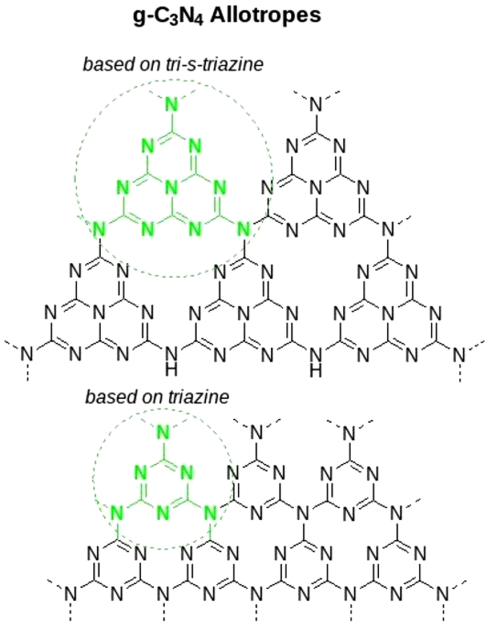

Figure 4: Graphitic carbon nitride triazine and tri-s-triazine allotropes structures. Based on ref. [75]. Copyright 2016, royal society of chemistry.

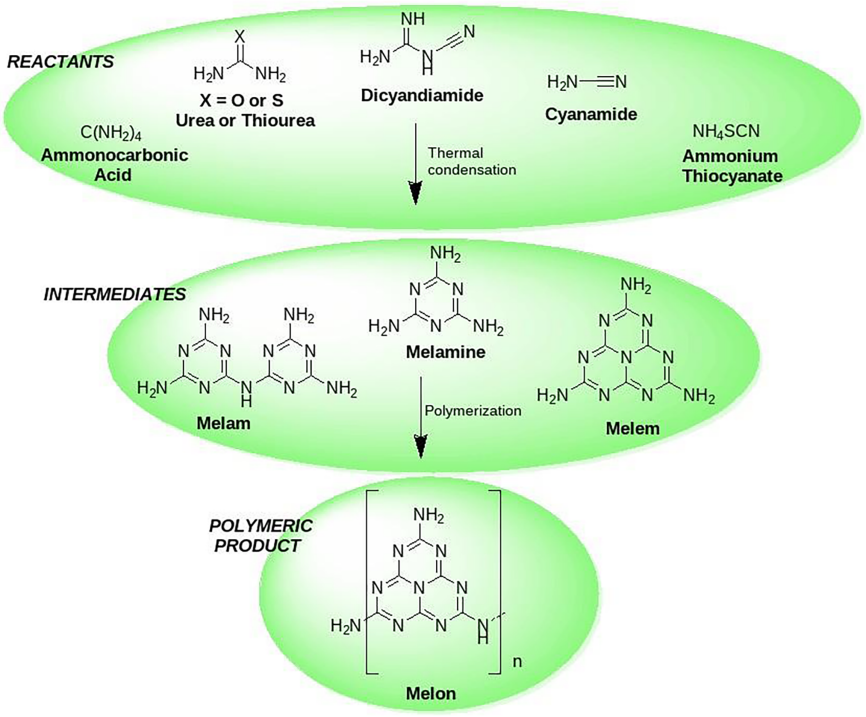

Figure 5: Synthetic approaches for obtaining g-C_3N_4 by thermal condensation. Based on ref. [83,84]. Copyright 2012, royal society of chemistry.

Concerning specific surface area, graphitic carbon nitride inherently possesses a high specific surface area, which can be further enhanced by suitable preparation methods. For example, the use of gas bubbles as a soft template can substantially increase the specific surface area [85].

Structural and morphological modifications are pivotal in broadening the application scope of g-C_3N_4 [86]. For instance, foam-like ultrathin carbon nitride nanosheets, prepared through sequential calcination of bulk g-C_3N_4 (synthetized by thermal condensation of melamine), provide enhanced photocatalytic efficiency, complementing strategies such as gas bubble templating. The resulting meso-, micro-, and macropores, along with cross-plane diffusion channels, enhance electron transport, charge separation, and photodegradation product removal [86]. The incorporation of Pt single atoms via this modification led to an approximately threefold enhancement in discharge capacity. At a current density of 100 $mA \cdot g^{-1}$, the modified batteries achieved discharge capacities nearly three times higher than those of the pristine support material without Pt single atoms. This finding underscores the propensity of graphitic carbon nitride to integrate heteroatoms, thereby enabling elevated atomic efficiency, a principle that likewise explains the prevalent use of nanoparticles in electrocatalytic and energy storage applications [87].

Although g-C_3N_4 consists of stacked bidimensional polymeric sheets primarily assembled by aromatic triazine/heptazine units, its conjugated aromatic molecular structure, characterized by the perpendicular-to-plane carbon p-orbitals conjugation, confers exceptional chemical and thermal stability, along with structural robustness. The rich nitrogen content generates low charge transfer, and the carbon nitride has little or no electron conductivity, being characterized as a semiconductor due to its band gap [88].

The photocatalytic activity of g-C_3N_4 originates from its polymeric semiconductor nature and distinctive electronic structure, which arises from the periodic arrangement of sp_2-hybridized C and N atoms in a framework within triazine and heptazine units. This framework forms an extended π-conjugated system through the overlap of p-orbitals, resulting in a valence band maximum (VBM) primarily composed of N 2p orbitals and a conduction band minimum (CBM) dominated by C 2p orbitals. The band gap of pristine g-C_3N_4 is typically reported in the range of 2.6–2.8 eV, enabling visible-light absorption up to approximately 460 nm [89].

Upon photon excitation with energy equal to or exceeding the band gap, electrons are excited from the valence to the conduction band, creating electron-hole pairs. These carriers drive surface redox reactions: the hydrogen evolution reaction (HER) reduces protons in aqueous media, while holes oxidize water or organic pollutants. A known limitation of this material is the rapid recombination of electron-hole pairs, caused by low electrical conductivity and high concentration of structural defects that act as recombination centers [90].

Recent research has demonstrated that the coupling of g-C_3N_4 with biomass-derived carbonaceous materials effectively mitigates this limitation while simultaneously enhancing the visible-light absorption. These improvements are primarily attributed to band gap narrowing, suppression of charge-carrier recombination, and more efficient interfacial charge transfer, ultimately leading to superior photocatalytic performance [91–95]. In this context, a hybrid photocatalyst composed of g-C_3N_4 and wheat straw–derived biochar (2% biochar/g-C_3N_4) was evaluated in the RhB degradation [94], achieving 91.3% RhB degradation efficiency after only 30 min of visible-light irradiation (Fig. 6a). The enhanced photocatalytic activity was primarily attributed to the improved visible-light absorption (band gap of 2.65 eV). The introduction of a small amount of biochar (2%) resulted in enhanced electron-transfer channels which effectively suppressed the recombination of photogenerated charge carriers on the g-C_3N_4 surface, with concomitant improvement in photocatalytic activity and recyclability of the catalyst [94].

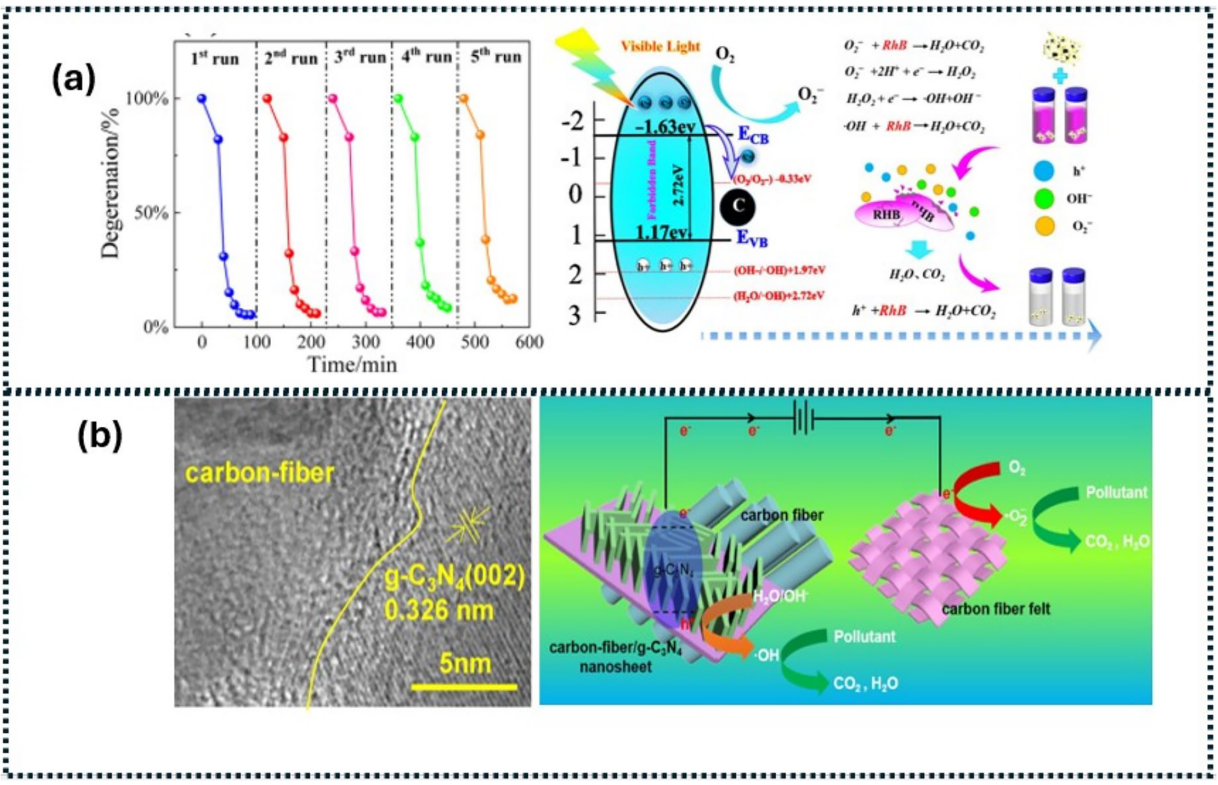

Figure 6: (**a**) HR-TEM morphology, band gap energy, and recyclability performance of biochar/g-C_3N_4 (2% CGCD), along with schematic diagram of the mechanism of photocatalytic degradation of RHB. (**b**) SEM micrographs, cycling stability, and schematic illustration of the photoelectrocatalytic system based on carbon-fiber/g-C_3N_4 nanosheets arrays. Reproduced with permission from refs. [94] (**a**), [93] (**b**).

The composite exhibited tailored optoelectronic properties, markedly enhanced visible-light absorption (band gap reduction from 2.77 to 2.62 eV), and a substantially lower charge recombination rate. As a result, outstanding methylene blue (MB) degradation efficiency (99.9%) was accomplished under visible-light irradiation [95]. When g-C_3N_4 is integrated with carbon nanofibers, photogenerated electrons can readily migrate from g-C_3N_4 nanosheets to the carbon fibers, thereby promoting efficient electron–hole separation and enhancing the photodegradation of organic contaminants [93]. The relevance of designing hybrids with g-C_3N_4 nanosheets was also demonstrated through the fabrication of carbon-fiber/g-C_3N_4 nanosheet arrays via chemical vapor deposition (Fig. 6b).

Owing to the favorable structural and electronic characteristics of the hybrid material, the authors successfully applied it in photoelectrocatalytic systems for environmental remediation and sustainable energy production. Notably, the degradation efficiency of 2,4-dinitrophenol reached an impressive 99.5% after 240 min of photoelectrocatalytic treatment.

Shafique et al. additionally investigated the photocatalytic behavior of g-C_3N_4 combined with algal biomass–derived biochar (g-C_3N_4@BC). The production of g-C_3N_4 and biopolymer hybrids has also been shown to effectively suppress charge recombination and enhance photocatalytic efficiency toward emerging contaminants, including bisphenol A [96], organic dyes [97], volatile organic compounds (VOCs) [98], pesticides such as imidacloprid (IMI), 2,4-dichlorophenoxyacetic acid (2,4-D) and atrazine (AZO), as well as antibiotics including tetracycline (TC), ofloxacin (OFX) and sulfadiazine (SDZ) [91,99]. Recently, biomass-derived carbon dots have been incorporated into g-C_3N_4 matrices due to their upconversion

photoluminescence properties, narrow band gap (~1.58 eV), and their ability to promote efficient separation and transfer of photogenerated charge carriers, particularly through $O_2\bullet^-$-mediated pathways. These features contribute to significantly enhanced photocatalytic performance in the degradation of emerging organic pollutants and other environmental remediation processes under visible light irradiation [100]. A metal-free photocatalyst based on CQDs/g-C_3N_4 composites obtained via calcination of a mixture of urea and carbon quantum dots was synthesized hydrothermally from discarded pine needles [100]. The composite exhibited markedly enhanced photocatalytic performance toward tetracycline (TC) degradation under visible-light irradiation (90.54% within 150 min) and natural solar light (93.5% within 10 min), displaying an apparent kinetic rate constant 12.6-fold higher than that of pristine g-C_3N_4. The superoxide radical ($O_2\bullet^-$) was identified as the dominant reactive species, while the material demonstrated high stability, good reusability (over five consecutive cycles), and a significant reduction in the toxicity of degradation intermediates. These findings highlight the strong potential of sustainable CQDs/g-C_3N_4 composites for the environmentally safe remediation of emerging organic contaminants in diverse aqueous matrices [100].

SACs supported on biomass and porous materials derived from sustainable routes have been extensively applied in photocatalysis, particularly in energy-related reactions and environmental remediation [101]. Despite the diversity of photocatalytic reactions and catalyst architectures reported, these studies collectively reveal recurring structure–activity relationships that transcend specific reactions or biomass sources. Fig. 7 summarizes the main photocatalytic applications of SACs, including hydrogen evolution, CO_2 reduction, and the degradation of organic pollutants. Fig. 7a shows H_2 production enabled by SACs supported on metal–organic frameworks (MOFs). The utilization of MOF MIL-25, as a metal-organic precursor, enabled an exceptionally high loading of isolated Cu atoms (~1.5 wt%) without significant aggregation [102]. This approach relied on the prior anchoring of Cu ions within the MIL-125 framework, promoting the formation of Cu–O–Ti bonds upon calcination, which ensured the uniform immobilization of metal atoms on the support. As a result, a stable atomic dispersion was achieved even at high loadings, facilitating efficient electron transfer through the Cu^{2+}/Cu^{+} redox pair. This architecture translated into superior photocatalytic performance for H_2 evolution under simulated solar irradiation, combined with a high apparent quantum efficiency (56%) and remarkable long-term stability (after 380 days of storage). This study illustrates that precise control of the coordination environment, rather than metal loading alone, is critical for achieving both high activity and long-term stability in photocatalytic SACs. Fig. 7b illustrates a sustainable photocatalytic strategy, in which biomass waste was converted into hydrothermal carbon (HTCC) for CO_2 reduction. By anchoring Cu species onto biomass-derived HTCC under hydrothermal conditions, Cu ions were effectively captured and reduced to metallic Cu, forming a Cu–HTCC photocatalyst. Owing to the favorable redox potential and catalytic activity of Cu, the resulting Cu–HTCC exhibited approximately twofold higher CO_2 reduction activity than pristine HTCC, achieving CO production rates ranging from 148.8 to 643.5 μmol g^{-1} h^{-1} [103]. Notably, this work highlights how biomass-derived supports can simultaneously act as carbon sources and coordination matrices, reducing synthetic complexity while maintaining competitive photocatalytic performance. Beyond energy-related reactions, SACs have been widely explored in advanced oxidation processes (AOPs) for the degradation of organic contaminants. The production of a biochar-based Fe–SAC was achieved from *Myriophyllum aquaticum* biomass and used for organic pollutant degradation [104]. The biochar was obtained through carbonization, activation, graphitization, and chemical etching, enabling the uniform deposition of isolated Fe atoms, reaching approximately 2.4 wt% of atomically dispersed Fe in the ISA Fe/MC catalyst. The ISA Fe/MC SAC was obtained via acid leaching (hydrochloric acid) of a nanostructured Fe/MC precursor, which transformed nanoparticulate Fe species into isolated Fe atoms stably anchored within the biochar matrix. The reported results demonstrated that isolated metal sites are particularly effective in advanced oxidation processes, where controlled redox cycling

and site accessibility govern radical generation efficiency. In the presence of peroxymonosulfate (PMS), the ISA Fe/MC catalyst enabled complete phenol removal within 6 min, with an apparent rate constant of 1.096 min^{-1}, underscoring the high catalytic efficiency of isolated Fe sites.

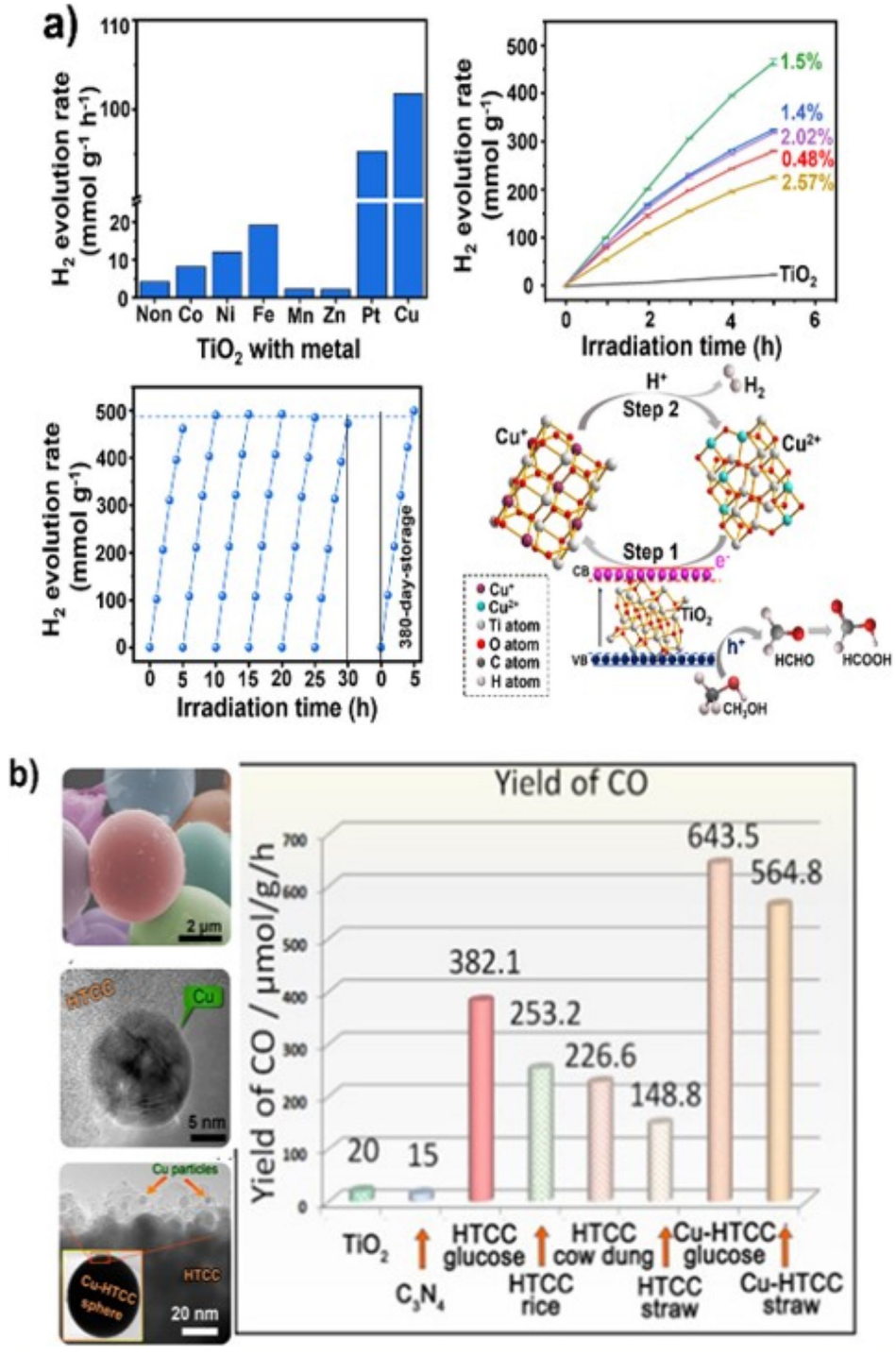

Figure 7: A schematic illustration of the versatile roles of single-atom catalysts (SACs) in photocatalysis. (**a**) SACs for photocatalytic H_2 evolution; and (**b**) SACs on biomass-derived carbon for CO_2 reduction. Reproduced with permission from refs. [102] Copyright 2025, Springer Nature (**a**) and [103] (**b**) Copyright © 2020 American Chemical Society.

An iron single-atom catalysts (Fe-SACs) was synthetized from iron-contaminated fern biomass collected during phytoremediation of iron mines [105]. The resulting Fe-SAC-800 exhibited outstanding activity and stability for peroxymonosulfate (PMS)-assisted photocatalytic degradation of quinolone antibiotics (norfloxacin [NOR], levofloxacin [LEV], ciprofloxacin [CIP], enrofloxacin [ENR], lomefloxacin [LOM], and flumequine [FLU]) under mild conditions, achieving near-complete removal efficiencies (>90%) and reaction rates markedly higher than those of previously reported photocatalysts. Advanced characterization techniques, including XAFS and HAADF-STEM, identified a well-defined Fe–N_4 coordination environment in the optimized Fe-SAC-800.

Despite these advances, a key limitation of SACs remains the difficulty in simultaneously achieving high metal loadings and long-term structural stability, as increasing metal content often promotes aggregation into clusters or nanoparticles. Consequently, many reported SACs exhibit relatively low metal loadings (typically 0.1–0.3 wt%), and maintaining atomic dispersion beyond ~0.5 wt% remains challenging. Additionally, strong interactions between reaction intermediates and isolated metal sites can lead to irreversible deactivation, compromising recyclability [106–108]. This inherent trade-off between atomic dispersion and metal loading remains one of the central bottlenecks for the practical deployment of SAC-based photocatalysts. To address these issues, recent efforts have focused on advanced support and coordination microenvironment engineering strategies that stabilize isolated atoms, regulate site–intermediate interactions, and preserve local coordination environments, thereby improving catalytic durability and performance [109,110]. In this context, a universal and green strategy for synthesizing carbon-based transition-metal SACs (M = Fe, Co, Ni, Cu, Zn) was reported via a one-pot hydrothermal treatment combined with a mechanochemical process [111]. This method exploits abundant anchoring sites in the carbon matrix and compression confinement to prevent metal aggregation during high-temperature pyrolysis, yielding monodispersed MO_3C atomic sites with metal loadings up to 1.15 wt%. Such strategies underscore the importance of confinement effects and defect-rich carbon matrices in overcoming aggregation at elevated metal loadings. The resulting Fe–SAC achieved 96.6% tetracycline removal under visible-light irradiation (Xe 300 W, 2 h), highlighting its superior photocatalytic efficiency, stability, and recyclability.

Further expanding biomass-derived SAC platforms, Cui et al. (2022) synthesized Mn–SACs by pyrolyzing *Phytolacca americana*, a Mn-hyperaccumulating plant, generating atomically dispersed Mn–N_4 sites within a porous carbon matrix with a Mn loading of approximately 1.2 wt% [112]. The catalyst achieved 99% degradation of rhodamine B (10 mg L^{-1}) within 60 min under visible light (300 W Xe lamp), with a rate constant of 0.052 min^{-1}, which is 6.5 times higher than that of TiO_2 P25, and retained its stability over 5 cycles. *In situ* XAS and DFT calculations confirmed that photoexcited electrons are transferred from adsorbed O_2 to the Mn–N_4 sites to generate $^1O_2$ (with a quantum efficiency of 98% at 420 nm), providing a cost-effective strategy to upcycle phytoremediated biomass into environmental catalysts. Similarly, Wang et al. (2020) employed nitrogen-rich cyanobacterial biomass to produce Cu–N/C SACs via molten salt–assisted pyrolysis, achieving 1.9 wt% atomically dispersed Cu and near-complete tetracycline removal over a wide pH range, demonstrating the versatility of biomass-derived SACs for environmental photocatalysis [107]. Nevertheless, the wide variation in synthesis routes, testing conditions, and performance metrics complicates direct comparison across studies, underscoring the need for standardized evaluation protocols. Collectively, these studies demonstrate that biomass-derived SACs provide a flexible and efficient platform for photocatalytic pollutant degradation, combining high atomic utilization, sustainable synthesis routes, and robust performance under visible-light irradiation.

2.4 Sustainable Carbon-Based Materials for Electrochemistry Applications

Electrochemical applications of biomass-derived carbon materials are governed by the same structure–property relationships discussed for heterogeneous catalysis and photocatalysis, particularly those related to heteroatom coordination, defect density, and electronic conductivity. Biomass-derived carbon nanomaterials thus represent a promising and sustainable platform for the development of high-performance and low-cost electrochemical systems. Their intrinsic heteroatom content, tunable pore architecture, and high specific surface area promote the formation of abundant electroactive sites, facilitating charge-transfer processes and enhancing catalytic activity [113–117]. Recent studies further demonstrate that the enhanced electrochemical performance of biomass-derived carbon-based sensors arises from synergistic interactions between the carbon matrix and incorporated dopants or nanoparticles, which collectively improve electrical conductivity, electroactive surface area, and charge-carrier mobility. In this context, the rational integration of heteroatoms, structural defects, and secondary nanophases emerges as an effective strategy to regulate charge-transfer pathways and expand the density and diversity of active sites.

To provide a comprehensive overview of recent advances, Table 2 summarizes key publications from the past few years covering sensor development, electrocatalysis, and other electrochemical applications. This compilation highlights the diversity of biomass precursors, dopants, structural engineering strategies, and performance metrics, helping identify emerging trends, recurring challenges, and promising research directions within the field of sustainable carbon-based catalysts. Numerous examples illustrate how structural and compositional tuning governs [118–127] electrochemical performance.

Table 2: Summary of biomass-derived carbon materials: synthesis routes, charge-transfer properties, and applications.

Material (Biomass Source)	Synthesis Route	Electrical Conductivity/Charger Transfer Indicator	Application	Representative Performance Metric	Ref.
Ag-modified sugarcane bagasse biochar	Pyrolysis	ECSA de 0.3 cm^2	Electrochemical detection of Hg^{2+}	LOD: 1.1 ppb	[118]
CeO_2·CuO@BC nanocomposite (biomass-derived C) (date seeds)	Pyrolysis	Rct de 12.8 kΩ/reduce the oxidation potential from +0.6 V to +0.45 V	Amperometric sensor for catechol	LOD: 0.035 μM	[119]
Fe-doped mesoporous carbon derived from pig blood	Pyrolysis	A steady state for H_2O_2 is reached within ~3 s	Electrochemical sensor for H_2O_2	LOD: 0.046 μM	[120]
MoO_3 nanoparticles with N-doped biomass-derived C (cow dung)	Pyrolysis	Rct de 0.822 kΩ	Portable electrochemical sensor for diclofenac	LOD: 0.08 μmol L^{-1}	[121]
Hierarchical porous C (plant-derived tannic acid)	Soft-hard dual-template and calcination	ECSA de 0.14 cm^2	Electrochemical detection of chlorogenic acid in herbs	LOD: 35.8 nM	[122]
Co-supported N, S-co-doped biochar	Cobalt loading on N, S co-doped biochar (from shrimp shells) via wet impregnation followed by pyrolysis.	TS for ORR: 35 mV dec^{-1}	Trifunctional electrocatalysis: ORR, OER and HER.	HER: η_{10} of 0.46 V at 10 mA cm^{-2}. OER: η_{10} of 0.57 V at 10 mA cm^{-2}. Stability (ORR): Current retention of 84.70% after 15 h.	[123]

(Continued)

Table 2 (continued)

Material (Biomass Source)	Synthesis Route	Electrical Conductivity/Charger Transfer Indicator	Application	Representative Performance Metric	Ref.
Porous Graphitic C Derived from Bagasse	Hydrothermal treatment	Rct de 16.9 Ω	Electrocatalysis of the ORR	Power density of the Zn–air battery of 191.9 mW cm^{-2} at 392 mA cm^{-2}	[124]
Coconut shell	Flash Joule Heating (FJH) at 3000°C with B nanolayers and melamine.	–	ORR for H_2O_2 synthesis	Productivity of 798 mmol g^{-1} catalyst h^{-1} (in a flow cell). Selectivity: 91%–94%. Faradaic efficiency: >80% over 11 h.	[125]
Mulberry peel	Pyrolysis	Rct of 3.1 Ω	Overall water splitting (HER/OER) in alkaline medium	η_{10} of 86 mV for HER. Cell voltage of 1.59 V at 10 mA cm^{-2} (two-electrode system).	[126]
Banana leaves	Pyrolysis		Water splitting (OER/HER) in alkaline medium	OER: −0.8 V. HER: 1.95 V (in 0.1 M KOH vs. RHE). H_2 production rate: 0.22 mL min, O_2 production rate: 0.078 mL min	[127]

For instance, silver-modified sugarcane bagasse biochar (SCBB@Ag) exhibited enhanced electron-transfer capability and improved selectivity toward Hg^{2+} detection due to the highly dispersed Ag nanoparticles [118]. In another work, a CeO_2·CuO@BC nanocomposite lowered the oxidation potential of catechol from +0.60 to +0.45 V, an effect attributed to its low charge-transfer resistance (Rct = 12.8 kΩ) and the presence of oxygen vacancies in the mixed-oxide lattice [119]. Structural optimization is also key: Jiang et al. (2023) prepared a hierarchical porous carbon using a soft–hard dual-template strategy with tannic acid as the precursor, obtaining a large electroactive surface area (0.14 cm^2) and an ultra low detection limit (LOD) of 6.2 nM for chlorogenic acid. Nitrogen doping and the incorporation of transition metal nanoparticles further enhance conductivity and reactivity. A nitrogen-doped carbon/molybdenum trioxide nanocomposite (CD–N/MoO_3) from cow dung, achieving excellent electrocatalytic activity and low detection limits for diclofenac (0.08 μmol L^{-1}) [121]. Pig-blood-derived carbon, whose intrinsic Fe centers and high graphitization degree (900°C) enabled hydrogen peroxide detection with a rapid response time (3 s). Collectively, these cases highlight how the interplay between dopants, hierarchical porosity, and graphitization degree governs charge transport and overall sensor sensitivity [120].

Biomass precursors bring clear sustainability advantages. Their inherent heteroatom content and natural porosity facilitate the formation of active sites and ion transport. However, the complex and heterogeneous composition of biomass often complicates structural control during pyrolysis, leading to irregular porosity, limited crystallinity, and hindered mass transport [128–130]. Dual-template strategies [122] mitigate these issues but add synthetic complexity. In addition, some biomass-derived carbons, especially those from lignin, straw, and agricultural residues, retain significant ash and silicate content after carbonization. Such mineral phases (e.g., SiO_2, Al_2O_3, alkaline oxides) can block pores, introduce electrochemically inactive domains, and impair electron transport, reducing electrochemical stability in alkaline media. Recent studies confirm that

rice husk-, straw- and lignin-derived carbons exhibit persistent mineral residues even after high-temperature pyrolysis, resulting in reduced conductivity and limited structural robustness [131,132]. Variability in ash and silica content among biomass sources further challenges the reproducibility and long-term stability of electrodes [133].

In summary, the renewable nature and intrinsic functionality of biomass make it an excellent carbon scaffold for electrochemical sensor design. However, achieving the crystallinity, porosity, and electrochemical stability required for next-generation sensing technologies demands precise control over precursor composition and carbonization parameters. A similar paradigm is observed in electrocatalysis. The catalytic performance of biomass-derived materials is governed by their structural, compositional, and electronic features, as well as by the deliberate incorporation of heteroatoms and metal species. Systematic studies show that pore architecture, graphitization degree, defect density, surface functionalization, and the presence of catalytically active metal centers critically influence charge-transfer kinetics, catalytic efficiency and operational stability. Guo et al. (2025) demonstrated that cotton-derived biochar modified with Ni and carbonates significantly improved coke resistance in the steam reforming of acetic acid, although partial surface-area loss and carbonate leaching remain problematic [134]. Transition-metal-doped carbons also exhibit multi-functional activity. Separately, Co/N, S co-doped biochar from shrimp shells showed trifunctional ORR/OER/HER performance, reaching an OER overpotential (η1) of 0.57 V at 10 mA cm^{-2}, comparable to IrO_2 [123]. Herein, ORR, OER, and HER refer to the oxygen reduction reaction, oxygen evolution reaction, and hydrogen evolution reaction, respectively. It is worth highlighting that the overpotential reported (η_{10} = 0.46 V) is relatively high compared to several transition metal/biochar composites described in the literature. The HER activity of the Co/N, S-CC and Fe/N, S-CC materials is attributed to the synergistic effect between the cobalt or iron species and the conductive N, S-co-doped carbon support. Furthermore, the incorporation of nitrogen and sulfur atoms into the carbon matrix modifies its electronic structure, thereby promoting hydrogen adsorption. In addition, N-doping enhances the hydrophobicity of the carbon-based catalyst, which improves electrode–electrolyte contact. The Tafel slope (TS) for the ORR was determined to be 35 mV dec^{-1}, indicating favorable reaction kinetics. A catalyst based on P/S self-doped carbon from coffee grounds, enabling selective $2e^-$ ORR for H_2O_2 production and efficient electrocatalytic degradation of Favipiravir [135]. Graphite-like porous carbon from sugarcane bagasse exhibiting a four-electron ORR pathway and high Zn–air battery power density (191.9 mW cm^{-2}) [124]. Xu et al. (2024) synthesized O/B/N-co-doped carbon from coconut shells, achieving 91%–94% H_2O_2 selectivity and >80% Faradaic efficiency for 11 h in flow cells [125]. This trend is further supported by recent reports on porous heteroatom-doped carbons derived from biomass for pH-universal H_2O_2 electroproduction, underscoring the importance of surface chemistry control in electrochemical systems [134]. Other notable biomass precursors include shrimp shells (Co_9S_8@N, P–carbon), legume root nodules, chicken feathers, banana leaves and water hyacinth, all yielding high ORR selectivity, low over potentials and excellent stability [123,136–139]. The main challenges across these systems include optimizing heteroatom and metal dopants, controlling nanoparticle size and distribution, tuning porosity and ensuring long-term stability in different electrolytes. For instance, excessive phosphorus doping may collapse the porous structure of Co_9S_8@NPC-10, while maintaining active-site integrity in acidic media for Mo/Fe self-doped catalysts requires careful retention of heteroatoms [123].

The physicochemical properties of biomass-derived carbons are strongly dictated by the nature of the precursor and the synthesis conditions. During pyrolysis, naturally occurring elements such as C, O, N, S, and P can promote self-doping, thereby eliminating the need for external dopants [134]. Nitrogen-rich precursors, including shrimp shells rich in chitin, have been widely explored for the production of heteroatom-doped porous carbons [139], while spent coffee grounds provide additional P- and S-containing functionalities suitable for catalytic and energy-related applications [140–142]. Similarly, keratin-containing

biomasses, such as chicken feathers, offer efficient routes toward N/S/O-doped carbons for electrochemical devices and energy storage systems [143,144]. By selecting appropriate precursors, researchers can fine-tune heteroatom content, electronic structure and the density of active sites. A hierarchical micro, meso and macroporous architecture is essential. Micropores supply a high electrochemically active surface area, whereas meso and macropores ensure efficient mass transport [140]. An optimal balance between porosity and graphitization is also required: graphitic domains enhance conductivity, while structural defects, often introduced via heteroatom doping, create active centers with modulated charge/spin density [141]. Rational design of porosity, doping and thermal treatment therefore enables simultaneous control of accessibility and catalytic activity, which is essential for high-performance electrocatalysts [142].

The electronic and synergistic effects of heteroatom dopants are central to defining activity and selectivity in ORR. Nitrogen doping (pyridinic-N, graphitic-N) is the most widely investigated, facilitating O_2 adsorption and stabilizing metal–N_x structures [143]. Boron doping generates electron-deficient sites that favor $2e^-$ ORR and H_2O_2 formation [144,145]. Hollow B-doped porous carbon spheres have achieved >90% H_2O_2 selectivity in alkaline media [144,145]. More complex systems, such as S-doped Co–N–C, benefit from synergistic interactions between S/N/metal centers, reaching half-wave potentials of 0.895 V vs. RHE (alkaline) [146]. N–S co-doped carbons also display enhanced active-site density and stability across pH values. Oxygen-containing groups (carbonyl, ether, hydroxy, carboxyl) increasingly emerge as key motifs for selective $2e^-$ ORR by stabilizing –OOH intermediates and suppressing O–O cleavage [146,147]. Beyond single dopants, co-doping and multi-heteroatom doping (N–S, N–P, N–B) produce strong charge polarization and defect engineering, improving ORR activity and selectivity between $2e^-$ and $4e^-$ pathways. When used as supports for transition-metal nanoparticles, heteroatom-doped carbons enhance metal–support interactions, leading to improved dispersion, accelerated electron transfer, and optimized adsorption of oxygenated intermediates [148,149].

Both studies demonstrate that biomass-derived carbon materials combined with cobalt-based active phases are highly effective for bifunctional electrocatalysis in water splitting. For instance, mulberry bark-derived carbon modified with cobalt phospho-boride achieved low overpotentials of −86 mV for HER and 310 mV for OER at 10 mA cm^{-2}, along with a low cell voltage of 1.59 V, demonstrating excellent overall water splitting performanc [126]. Similarly, banana leaf-derived N-doped porous carbon embedded with cobalt nanoparticles exhibited high gas evolution rates of 0.22 mL min^{-1} for H_2 (at −0.8 V vs. RHE) and 0.078 mL min^{-1} for O_2 (at 1.95 V vs. RHE) in 0.1 M KOH, highlighting its catalytic efficiency [127]. These findings confirm that the synergistic interaction between biomass-derived carbon frameworks and cobalt-based species, either as nanoparticles or phospho-boride phases, plays a crucial role in enhancing catalytic activity, stability, and charge transfer, reinforcing their potential for cost-effective green hydrogen production.

These shared descriptors suggest that design principles established in catalysis and photocatalysis can be directly translated to electrochemical systems, highlighting significant opportunities for future cross-disciplinary development. In summary, the interplay among dopant type, co-doping strategy, defect formation, and electronic structure is decisive for tuning catalytic activity, stability and selectivity toward H_2O_2 or H_2O. Rational catalyst design, guided by desired ORR pathways, electrolyte conditions, and application requirements, remains essential for advancing metal-free or low-metal electrocatalysts.

3 Biomass Carbon-Based Materials Characterization—Challenges and Advances

The characterization of carbon-based materials has some critical aspects inherent to their structural variety, including crystalline forms (diamonds and graphite), amorphous carbon (amorphous carbon and diamond like carbon, DLC), and nanostructured carbon (CNT, graphene, fullerenes). These materials exhibit varied hybridization (sp^2 and sp^3), disorder, complex porosity, low density, and chemical heterogeneity,

imposing challenges in their precise characterization. The intrinsic compositional variability of biomass feedstocks directly affects catalyst structure and performance, leading to reproducibility challenges across laboratories and limiting the transferability of laboratory-scale results to larger-scale applications. To mitigate these issues, recommended strategies include feedstock pre-classification, tighter control of processing parameters, and standardized reporting of synthesis and characterization conditions, which together can improve reproducibility and enable more reliable cross-study comparison.

Regarding structural features, most of the carbon produced from sustainable sources is amorphous, with an absence of structural order. X-ray diffraction (XRD) is the primary tool for the determination of the structure of materials. However, this disorder produces diffractograms with broad peaks, making phase distinction and the detailed quantification complex. Beyond these intrinsic limitations, XRD is inherently limited in the spatial resolution required to directly identify isolated metal atoms, rendering individual active sites in low-loading SACs (<2 wt%) effectively undetectable [150]. Consequently, SAC characterization relies on complementary techniques that, while informative, often provide qualitative or statistically limited insights due to low metal concentrations and the dynamic evolution of active sites under reaction conditions [151]. As a result, the quantitative discrimination between isolated and aggregated metal species, particularly under *in situ*/operando conditions, remains a critical challenge. Addressing this limitation will require integrated multimodal characterization frameworks, tightly coupled with advanced theoretical modeling, to enable a robust and predictive understanding of SAC structure–performance relationships [152].

With regard to the characterization by High Resolution Transmission Electron Microscopy (HRTEM) some relevant hurdles must be overcome in the characterization of carbon materials. Carbon, characterized by its low atomic number (Z = 6), behaves as a weak electron-scattering material, giving rise to the so-called contrast–voltage paradox; consequently, the characterization of carbon-based structures, such as graphene, carbon nanotubes, organic thin films, carbon nitride (e.g., graphitic g-C_3N_4), activated carbon, biochar, carbon black, and mesoporous carbons by conventional HRTEM is particularly challenging due to the combined effects of low scattering cross-sections and beam-induced radiation damage. At standard high accelerating voltages (200–300 kV), the elastic scattering cross-section is minimal, leading to poor image contrast. Modern methodologies emphasizes reducing the acceleration voltage to 60–80 kV (and progressively to 30 kV). This reduction increases the electron-matter interaction probability, significantly enhancing the contrast required to resolve the atomic lattice of light elements.

A further limitation in imaging sp^2-hybridized carbon is knock-on damage, as the displacement threshold is approximately 86 keV [153], imposing a critical constraint on maintaining structural integrity during HRTEM analysis. Operating at the common 200 or 300 kV levels exceeds this energy threshold, causing direct kinetic displacement of carbon atoms and rapid structural degradation. Utilizing low-voltage regimes is therefore essential for "damage-free" imaging, preserving the sample's intrinsic configuration during observation. Historically, lowering the voltage resulted in a drastic loss of resolution due to the dominance of spherical and chromatic aberrations. However, the development of aberration-corrected microscopes over the last two decades has revolutionized this field. Advanced spherical aberration correctors enable high-precision imaging at low accelerating voltages, allowing modern instruments to maintain sub-angstrom resolution even at 60 kV by compensating for geometric aberrations that would otherwise degrade image sharpness [154]. While standard field emission gun (FEG) systems, which works at 200 kV, remains the most cost-effective and common configuration [154], they are often suboptimal for light-element research. Without the specific tuning and correction hardware of high-end platforms, standard 200 kV systems fail to provide the delicate balance of high contrast and structural preservation required for carbon-based nanotechnology. The gold standard for carbon research has shifted toward low-voltage,

aberration-corrected TEM/STEM. Although conventional 200 kV FEG TEMs still provide substantial structural and compositional information on carbon-based nanostructures used in catalysis, recent advances in aberration-corrector technology over the past decade now enable atomic-scale visualization of light-element frameworks while operating below the threshold for radiation-induced damage.

Finally, the complexity of a porous network with a high density of micropores also poses significant challenges in determining the specific surface area (SSA) through gas physisorption. Although N_2 physisorption has been widely used for SSA determination, several critical factors must be considered. One of these concerns sample pretreatment: while mesoporous materials typically require high temperatures (e.g., 300°C) for a short period, the pretreatment of microporous materials generally involves longer times at lower temperatures (e.g., 200°C–250°C) to avoid structural damage while addressing diffusional limitations. Furthermore, the application of the BET method to such data is not always advisable, as the monolayer capacity may be inaccurately estimated due to micropore filling occurring in the same low relative pressure region as monolayer-multilayer adsorption. The choice of mathematical model for calculations remains a topic of ongoing debate, and the utilization of density functional theory (DFT)-based approaches (e.g., NLDFT or QSDFT) has been proposed to better reflect the complexity of porous networks [155]. Additionally, the utilization of smaller probe molecules, such as argon (Ar) and krypton (Kr), instead of nitrogen (N_2), has also been employed for SSA determination. The use of Ar at 87 K is indeed recommended by the International Union of Pure and Applied Chemistry (IUPAC) (2015 technical report) [145] as the preferred adsorbate for the determination of surface area and pore size analysis in many microporous materials, particularly those with polar surfaces. For microporous carbons (generally non-polar), both N_2 at 77 K and Ar at 87 K are suitable and widely employed, yielding comparable results. From a kinetic perspective, Ar at 87 K offers advantages, as micropore filling occurs at higher relative pressures, facilitating faster diffusion and more rapid attainment of equilibrium. Nevertheless, the IUPAC report highlights that both Ar and N_2 exhibit kinetic limitations at cryogenic temperatures (87 and 77 K), restricting their applicability for very narrow micropores (ultramicropores). To address this issue, the use of CO_2 as the adsorbate at 273 K is recommended. At this temperature, the higher saturation vapor pressure of CO_2 (approximately 3.5 MPa or ~26,000 Torr) enables much faster diffusion and access to very narrow pores (down to ~0.4 nm). The utilization of CO_2 has been widely employed for the characterization of narrow microporosity in carbonaceous materials, although it is not recommended for microporous solids with polar surface groups due to its strong quadrupole moment.

Aside from the molecule choice, it must be emphasized once again that the pretreatment (outgassing) stage requires particular care to ensure accurate and reproducible measurements. For microporous materials, including carbons, outgassing should be performed under high vacuum (typically <1 Pa) to effectively remove pre-adsorbed species without causing structural damage. Excessive temperatures or prolonged exposure can lead to pore collapse or chemical alterations in sensitive carbons, while insufficient outgassing may result in incomplete removal of adsorbates, underestimating the accessible porosity.

4 Conclusions

The utilization of biomass for the production of porous carbon offers a sustainable and environmentally benign pathway for advancing applications in heterogeneous catalysis, photocatalysis, and electrochemistry. By adopting a unified comparative framework, this review highlights how common design principles and constraints shape the performance of biomass-derived carbon catalysts across different catalytic platforms, thereby enabling more effective cross-disciplinary insight and rational material development.

These materials, derived from abundant renewable sources such as agricultural residues, facilitate waste valorization while providing high specific surface areas, hierarchical porosity, and intrinsic heteroatom

doping, which are essential for enhanced catalytic performance, efficient mass transport, and improved charge transfer.

Nevertheless, to ensure that the synthesis is truly sustainable, critical aspects of the entire biomass conversion pathway must be addressed, including the environmental impact of reactants, generated gases, and solid wastes. Energy consumption, cost-efficiency, and process scalability require careful evaluation. Furthermore, optimization should prioritize the local availability of sustainable raw materials to minimize transportation issues, particularly given the low density of vegetal biomass.

Another critical aspect is related to the absence of standard methodologies for the treatment and conversion of biomass, which imposing serious regulatory concerns. Ongoing advancements in greener activation techniques, precise doping strategies, and comprehensive life-cycle assessments hold promise for overcoming these limitations, ultimately reinforcing the role of biomass-derived porous carbons in promoting circular economy principles and sustainable technological progress in energy and environmental fields.

Moreover, biomass utilization creates a new value chain for agricultural and other biomass byproducts, supporting circular economy principles. As research progresses, international collaboration between these biomass-rich nations could accelerate the optimization of conversion processes and the scale-up of production. Future efforts should focus on standardizing protocols for biomass conversion, characterization methods (biomass as a raw material and the produced porous carbon) and establishing pilot projects to demonstrate the commercial viability of these sustainable materials, particularly in developing agricultural economies where the greatest socioeconomic impact will take place.

Acknowledgement: The authors thank the Microscopy Laboratory (LABMI) of the National Institute of Metrology, Quality, and Technology and Instituto Nacional de Metrologia, Qualidade e Tecnologia for technical support.

Funding Statement: The authors are grateful for the financial support provided by the Conselho Nacional de Desenvolvimento Científico e Tecnológico (CNPq, Brazil) and the Fundação Carlos Chagas Filho de Amparo à Pesquisa do Estado do Rio de Janeiro (FAPERJ).

Author Contributions: Authors confirm contributions to the text as follows: Kelly Leite dos Santos Castro Assis: Writing—review & editing, Visualization, Conceptualization; Druval Santos de Sá: review & editing, Visualization, Conceptualization; Bruno da Silva Marques: review & editing, Visualization, Conceptualization. Carolina Carvalho de Mello: review & editing, Visualization; João Lucas Marques Barros: Writing—original draft; Henrique Carvalhais Milanezi: Writing—original draft; João Batista Oliveira dos Santos: Writing—review & editing; Carlos Alberto Franchini: Writing—review & editing, Conceptualization, Writing—original draft. Bráulio Soares Archanjo: Resources, Writing—review & editing. Carlos Alberto Achete: Supervision, Resources, Project administration, Writing—review & editing, Funding acquisition; Adriana Maria da Silva: Writing—review & editing, Supervision, Resources, Project administration, Funding acquisition. All authors reviewed and approved the final version of the manuscript.

Availability of Data and Materials: No datasets were generated or analyzed during the current study.

Ethics Approval: Not applicable.

Conflicts of Interest: The authors declare no conflicts of interest.

References

1. Savova D, Apak E, Ekinci E, Yardim F, Petrov N, Budinova T, et al. Biomass conversion to carbon adsorbents and gas. Biomass Bioenergy. 2001;21(2):133–42. doi:10.1016/S0961-9534(01)00027-7.
2. da Costa GG, dos Santos IFS, Barros RM, Tiago Filho GL, de Oliveira Machado G, Barbedo MDG. Mapping and energy analysis of Brazilian bioenergy power potential for three agricultural biomass byproducts. J Clean Prod. 2022;349(6):131466. doi:10.1016/j.jclepro.2022.131466.

3. Chakroborty S, Pal K, Nath N, Singh V, Barik A, Soren S, et al. Sustainable synthesis of multifunctional nanomaterials from rice wastes: a comprehensive review. Environ Sci Pollut Res. 2023;30(42):95039–53. doi:10.1007/s11356-023-29235-9.
4. Yu K, Wang J, Wang X, Liang J, Liang C. Sustainable application of biomass by-products: corn straw-derived porous carbon nanospheres using as anode materials for lithium ion batteries. Mater Chem Phys. 2020;243:122644. doi:10.1016/j.matchemphys.2020.122644.
5. Kettum W, Samart C, Chanlek N, Pakawanit P, Reubroycharoen P, Guan G, et al. Enhanced adsorptive composite foams for copper (II) removal utilising bio-renewable polyisoprene-functionalised carbon derived from coconut shell waste. Sci Rep. 2021;11(1):1459. doi:10.1038/s41598-020-80789-x.
6. Maluin FN, Hussein MZ, Idris AS. An overview of the oil palm industry: challenges and some emerging opportunities for nanotechnology development. Agronomy. 2020;10(3):356. doi:10.3390/agronomy10030356.
7. Schwidtal JM, Piccini P, Troncia M, Chitchyan R, Montakhabi M, Francis C, et al. Emerging business models in local energy markets: a systematic review of peer-to-peer, community self-consumption, and transactive energy models. Renew Sustain Energy Rev. 2023;179:113273. doi:10.1016/j.rser.2023.113273.
8. Wang Y, Zhang M, Shen X, Wang H, Wang H, Xia K, et al. Biomass-derived carbon materials: controllable preparation and versatile applications. Small. 2021;17(40):2008079. doi:10.1002/smll.202008079.
9. Ge L, Zuo M, Wang Y, Wang R, Rong N, Qi Z, et al. A review of comprehensive utilization of biomass to synthesize carbon nanotubes: from chemical vapor deposition to microwave pyrolysis. J Anal Appl Pyrolysis. 2024;177:106320. doi:10.1016/j.jaap.2023.106320.
10. Zhang M, Zhang J, Ran S, Sun W, Zhu Z. Biomass-Derived sustainable carbon materials in energy conversion and storage applications: status and opportunities. A mini review. Electrochem Commun. 2022;138(2014):107283. doi:10.1016/j.elecom.2022.107283.
11. Vinod A, Pulikkalparambil H, Jagadeesh P, Rangappa SM, Siengchin S. Recent advancements in lignocellulose biomass-based carbon fiber: synthesis, properties, and applications. Heliyon. 2023;9(3):e13614. doi:10.1016/j.heliyon.2023.e13614.
12. Belluati M, Tabasso S, Calcio Gaudino E, Cravotto G, Manzoli M. Biomass-derived carbon-based catalysts for lignocellulosic biomass and waste valorisation: a circular approach. Green Chem. 2024;26(15):8642–68. doi:10.1039/d4gc00606b.
13. Wang Z, Shen D, Wu C, Gu S. State-of-the-art on the production and application of carbon nanomaterials from biomass. Green Chem. 2018;20(22):5031–57.
14. Deng J, Li M, Wang Y. Biomass-derived carbon: synthesis and applications in energy storage and conversion. Green Chem. 2016;18(18):4824–54. doi:10.1039/c6gc01172a.
15. Zhou Y, He J, Chen R, Li X. Recent advances in biomass-derived graphene and carbon nanotubes. Mater Today Sustain. 2022;18(8):100138. doi:10.1016/j.mtsust.2022.100138.
16. Albers PW, Pietsch J, Krauter J, Parker SF. Investigations of activated carbon catalyst supports from different natural sources. Phys Chem Chem Phys. 2003;5(9):1941–9. doi:10.1039/b212210n.
17. Jüntgen H. Activated carbon as catalyst support. Fuel. 1986;65(10):1436–46. doi:10.1016/0016-2361(86)90120-1.
18. Wang Y, Zhao Z, Zhao Y, Lan X, Xu W, Chen L, et al. A ZrO_2-RGO composite as a support enhanced the performance of a Cu-based catalyst in dehydrogenation of diethanolamine. RSC Adv. 2019;9(52):30439–47. doi:10.1039/c9ra05458h.
19. Mignoli TR, Hewer TLR, Alves RMB, Schmal M. Reduced graphene oxide (rGO) as new support of cobalt/lanthanum oxide for the water gas shift reaction (WGSR). Appl Catal A Gen. 2022;635:118553. doi:10.1016/j.apcata.2022.118553.
20. Barros JLM, Nunes MM, Alves OC, Franchini CA, Corat EJ, Silva AM. Evaluation of Al_2O_3 and ZrO_2 addition to reduced graphene oxide (rGO) supports and their interplay with Cu sites in the catalyst surface. Inorg Chem Commun. 2022;142(14):109591. doi:10.1016/j.inoche.2022.109591.
21. Franchini CA, Llorca J, Kuznetsov A, Silva AM. Outstanding dispersion of CeO_2 on reduced graphene oxide. Implications for highly dispersed Pd catalysts. Diam Relat Mater. 2020;109(2527):108061. doi:10.1016/j.diamond.2020.108061.

22. Pitínová M, Danylo I, Shafiq A, Hartman T, Khover M, Sevemez B, et al. Graphene oxide-supported metal catalysts for selective hydrogenation of cinnamaldehyde: impact of metal choice and support structure. Catalysts. 2025;15(5):470. doi:10.3390/catal15050470.
23. Dandia A, Gupta SL, Saini P, Sharma R, Meena S, Parewa V. Structure couture and appraisal of catalytic activity of carbon nitride (g-C_3N_4) based materials towards sustainability. Curr Res Green Sustain Chem. 2020;3:100039. doi:10.1016/j.crgsc.2020.100039.
24. Ashok A, Kumar A. Atomic level transition of graphene layer to carbon nanotubes over cobalt during ethanol decomposition reaction. Int J Hydrogen Energy. 2024;75:121–31. doi:10.1016/j.ijhydene.2024.01.070.
25. Cinnathambi Subramani M, Budiman I, Subyakto S, Chitraningrum N, Pari G, Widyaningrum BA, et al. A review on functionalized carbon nanotubes as a heterogeneous catalyst for the synthesis of one-pot multicomponent reactions. J Organomet Chem. 2025;1038:123767. doi:10.1016/j.jorganchem.2025.123767.
26. De Luca P, Siciliano C, Nagy JB, Macario A. The role of carbon nanotubes in the reactions of heterogeneous catalysis. Chem Eng Res Des. 2023;197(1–2):74–84. doi:10.1016/j.cherd.2023.07.016.
27. de Oliveira JPB, Iwasaki MT, Milanezi HC, Barros JLM, Simionato AA, da Silva Marques B, et al. Production of sustainable synthetic natural gas from carbon dioxide and renewable energy catalyzed by carbon-nanotube-supported Ni and ZrO_2 nanoparticles. Catalysts. 2025;15(7):675. doi:10.3390/catal15070675.
28. Sengel SB, Deveci H, Bas H, Butun V. Carbon spheres as an efficient green catalysts for dehydrogenation of sodium borohydride in methanol. Catal Commun. 2023;177(8):106650. doi:10.1016/j.catcom.2023.106650.
29. Molefe T, Jiang Y, Magubane A, Mguni L, Sikeyi L, Jiang C, et al. Hollow carbon spheres as catalyst support for Fischer-Tropsch synthesis: synthesis techniques, optimization strategies, and future research. Fuel Process Technol. 2025;276:108285. doi:10.1016/j.fuproc.2025.108285.
30. Zhang SZ, Cui ZS, Zhang M, Zhang ZH. Biochar-based functional materials as heterogeneous catalysts for organic reactions. Curr Opin Green Sustain Chem. 2022;38:100713. doi:10.1016/j.cogsc.2022.100713.
31. Balajii M, Niju S. Biochar-derived heterogeneous catalysts for biodiesel production. Environ Chem Lett. 2019;17(4):1447–69. doi:10.1007/s10311-019-00885-x.
32. Jaryal VB, Villa A, Gupta N. Metal-free carbon-based nanomaterials: insights from synthesis to applications in sustainable catalysis. ACS Sustainable Chem Eng. 2023;11(41):14841–65.
33. Liu J. Catalysis by supported single metal atoms. ACS Catal. 2017;7(1):34–59. doi:10.1021/acscatal.6b01534.
34. Chauhan A, Srivastava R. Biomass valorization with metal-free catalysts: innovations in thermocatalytic, photocatalytic, and electrocatalytic approaches. Chem Soc Rev. 2025;54(15):7114–73. doi:10.1039/d5cs00304k.
35. Polidoro D, Perosa A, Selva M, Rodríguez-Padrón D. Metal-free carbonaceous catalytic materials: biomass feedstocks for a greener future. ChemCatChem. 2023;15(13):e202300415. doi:10.1002/cctc.202300415.
36. Xiong W, Wang Z, He S, Hao F, Yang Y, Lv Y, et al. Nitrogen-doped carbon nanotubes as a highly active metal-free catalyst for nitrobenzene hydrogenation. Appl Catal B Environ. 2020;260(3):118105. doi:10.1016/j.apcatb.2019.118105.
37. Lang M, Wang D, Yang S, Li H. N-S vacancy sites on heteroatomic doping metal-free carbo-catalyst for efficient biomass hydrodeoxygenation. Fuel. 2024;366(21):131222. doi:10.1016/j.fuel.2024.131222.
38. Rangraz Y, Heravi MM. Recent advances in metal-free heteroatom-doped carbon heterogonous catalysts. RSC Adv. 2021;11(38):23725–78. doi:10.1039/d1ra03446d.
39. Yang S, Xu S, Tong J, Ding D, Wang G, Chen R, et al. Overlooked role of nitrogen dopant in carbon catalysts for peroxymonosulfate activation: intrinsic defects or extrinsic defects? Appl Catal B Environ. 2021;295:120291. doi:10.1016/j.apcatb.2021.120291.
40. Cao Y, Mao S, Li M, Chen Y, Wang Y. Metal/porous carbon composites for heterogeneous catalysis: old catalysts with improved performance promoted by N-doping. ACS Catal. 2017;7(12):8090–112. doi:10.1021/acscatal.7b02335.
41. Li Z, Huang Y, Chi X, Li D, Zhong L, Li X, et al. Biomass-based N doped carbon as metal-free catalyst for selective oxidation of d-xylose into d-xylonic acid. Green Energy Environ. 2022;7(6):1310–7. doi:10.1016/j.gee.2021.01.004.
42. Pérez Mayoral E, Godino Ojer M, Ventura M, Matos I. New insights into N-doped porous carbons as both heterogeneous catalysts and catalyst supports: opportunities for the catalytic synthesis of valuable compounds. Nanomaterials. 2023;13(13):2013. doi:10.3390/nano13132013.

43. Hu X, Fan M, Zhu Y, Zhu Q, Song Q, Dong Z. Biomass-derived phosphorus-doped carbon materials as efficient metal-free catalysts for selective aerobic oxidation of alcohols. Green Chem. 2019;21(19):5274–83.
44. Kilic A, Aytar E, Kleij AW. Boron catalysis to expedite the synthesis of organic carbonates from carbon dioxide. ChemCatChem. 2025;17(7):e202500002. doi:10.1002/cctc.202500002.
45. Zhang R, Shehzad N, Zhang L, Bin A, Shahid I. Investigating the synergistic effect of sulfur and nitrogen co-doping in graphene for enhanced CO_2 reduction to CO: a computational study. Diam Relat Mater. 2023;139:110310. doi:10.1016/j.diamond.2023.110310.
46. Mei S, Gu J, Ma T, Li X, Hu Y, Li W, et al. N-doped activated carbon from used dyeing wastewater adsorbent as a metal-free catalyst for acetylene hydrochlorination. Chem Eng J. 2019;371:118–29. doi:10.1016/j.cej.2019.04.008.
47. Qiao B, Wang A, Yang X, Allard LF, Jiang Z, Cui Y, et al. Single-atom catalysis of CO oxidation using Pt1/FeO_x. Nat Chem. 2011;3(8):634–41. doi:10.1038/nchem.1095.
48. Yang XF, Wang A, Qiao B, Li J, Liu J, Zhang T. Single-atom catalysts: a new frontier in heterogeneous catalysis. Acc Chem Res. 2013;46(8):1740–8. doi:10.1021/ar300361m.
49. Korampattu L, Dhepe PL. Nitrogen doped carbon supported ruthenium catalyst from chitosan: a sustainable approach for efficient hydrogenation of Levulinic acid to γ-valerolactone [Internet]. 2025 [cited 2026 Jan 1]. Available from: https://chemrxiv.org/doi/full/10.26434/chemrxiv-2025-njbzq.
50. Yu N, Liu X, Kuai L. Natural biomass derived single-atom catalysts for energy and environmental applications. Int J Biol Macromol. 2024;276(Pt 1):133694. doi:10.1016/j.ijbiomac.2024.133694.
51. Gawande MB, Fornasiero P, Zbořil R. Carbon-based single-atom catalysts for advanced applications. ACS Catal. 2020;10(3):2231–59. doi:10.1021/acscatal.9b04217.
52. Li J, Wang G, Sui W, Parvez AM, Xu T, Si C, et al. Carbon-based single-atom catalysts derived from biomass: fabrication and application. Adv Colloid Interface Sci. 2024;329:103176. doi:10.1016/j.cis.2024.103176.
53. Zhang F, Yang X, Guan J, Qiu J. Biomass-based single-atom catalysts: synthesis, structure regulation, and applications in energy conversion. Nano Res. 2025;18(12):94907865. doi:10.26599/nr.2025.94907865.
54. Gao S, Li M, Li N, Zhang L, Liu Q, Wang X, et al. Porous carbon-nanostructured electrocatalysts for zinc–air batteries: from materials design to applications. Nanoscale Adv. 2025;7(1):60–88. doi:10.1039/d4na00847b.
55. Rivera-Cárcamo C, Serp P. Single atom catalysts on carbon-based materials. ChemCatChem. 2018;10(22):5058–91. doi:10.1002/cctc.201801174.
56. Zhou H, Xu H, Liu Y. Aerobic oxidation of 5-hydroxymethylfurfural to 2,5-furandicarboxylic acid over Co/Mn-lignin coordination complexes-derived catalysts. Appl Catal B Environ. 2019;244(20):965–73. doi:10.1016/j.apcatb.2018.12.046.
57. Zhou H, Hong S, Zhang H, Chen Y, Xu H, Wang X, et al. Toward biomass-based single-atom catalysts and plastics: highly active single-atom Co on N-doped carbon for oxidative esterification of primary alcohols. Appl Catal B Environ. 2019;256:117767. doi:10.1016/j.apcatb.2019.117767.
58. Matos I, Silva MF, Ruiz-Rosas R, Vital J, Rodríguez-Mirasol J, Cordero T, et al. Methoxylation of α-pinene over mesoporous carbons and microporous carbons: a comparative study. Microporous Mesoporous Mater. 2014;199(6):66–73. doi:10.1016/j.micromeso.2014.08.006.
59. Akbayrak S, Özçifçi Z, Tabak A. Activated carbon derived from tea waste: a promising supporting material for metal nanoparticles used as catalysts in hydrolysis of ammonia borane. Biomass Bioenergy. 2020;138(2):105589. doi:10.1016/j.biombioe.2020.105589.
60. Benedetti V, Ail SS, Patuzzi F, Cristofori D, Rauch R, Baratieri M. Investigating the feasibility of valorizing residual char from biomass gasification as catalyst support in Fischer-Tropsch synthesis. Renew Energy. 2020;147:884–94. doi:10.1016/j.renene.2019.09.050.
61. Nemati B, Kamali M, Aminabhavi TM, Dewil R, Ferreira P, Silva MRF, et al. Production of high yield and high-quality carbon nanotubes from biomass wastes under microwave irradiation—mechanism and properties. Sustain Mater Technol. 2025;45:e01573. doi:10.1016/j.susmat.2025.e01573.
62. Zhang M, Hu C, Li N, Zhang Y, Khodakov A, Zhang Y, et al. Low temperature glycerol steam reforming on Ni/CNTs catalysts: the effect of nano-confinement. Int J Hydrogen Energy. 2024;91:1253–61. doi:10.1016/j.ijhydene.2024.10.181.

63. Seelam PK, Huuhtanen M, Sápi A, Szabó M, Kordás K, Turpeinen E, et al. CNT-based catalysts for H_2 production by ethanol reforming. Int J Hydrogen Energy. 2010;35(22):12588–95. doi:10.1016/j.ijhydene.2010.07.160.
64. Rong C, Flint K, Doonan C, Chen Y. Recent advances in high-loading single-atom catalysts. Next Mater. 2025;7:100457. doi:10.1016/j.nxmate.2024.100457.
65. Jin Y, Tang W, Wang J, Chen Z, Ren F, Sun Z, et al. High photocatalytic activity of spent coffee grounds derived activated carbon-supported Ag/TiO_2 catalyst for degradation of organic dyes and antibiotics. Colloids Surf A Physicochem Eng Aspects. 2022;655:130316. doi:10.1016/j.colsurfa.2022.130316.
66. Kamran U, Lee SY, Rhee KY, Park SJ. Rice husk valorization into sustainable Ni@TiO_2/biochar nanocomposite for highly selective Pb (II) ions removal from an aqueous media. Chemosphere. 2023;323:138210. doi:10.1016/j.chemosphere.2023.138210.
67. Zafeer MK, Menezes RA, Venkatachalam H, Bhat KS. Sugarcane bagasse-based biochar and its potential applications: a review. Emergent Mater. 2024;7(1):133–61. doi:10.1007/s42247-023-00603-y.
68. Yuan L, Shao C, Zhang Q, Webb E, Zhao X, Lu S. Biomass-derived carbon dots as emerging visual platforms for fluorescent sensing. Environ Res. 2024;251:118610. doi:10.1016/j.envres.2024.118610.
69. Mergbi M, Galloni MG, Aboagye D, Elimian E, Su P, Ikram BM, et al. Valorization of lignocellulosic biomass into sustainable materials for adsorption and photocatalytic applications in water and air remediation. Environ Sci Pollut Res Int. 2023;30(30):74544–74. doi:10.1007/s11356-023-27484-2.
70. Zhou H, Pan J, Ding L, Tang Y, Ding J, Guo Q, et al. Biomass-derived hierarchical porous CdS/M/TiO_2 (M = Au, Ag, Pt, Pd) ternary heterojunctions for photocatalytic hydrogen evolution. Int J Hydrogen Energy. 2014;39(29):16293–301. doi:10.1016/j.ijhydene.2014.08.032.
71. Mian MM, Liu G. Recent progress in biochar-supported photocatalysts: synthesis, role of biochar, and applications. RSC Adv. 2018;8(26):14237–48. doi:10.1039/c8ra02258e.
72. Zhao H, Cheng Y, Liu W, Yang L, Zhang B, Wang LP, et al. Biomass-derived porous carbon-based nanostructures for microwave absorption. Nano Micro Lett. 2019;11(1):24. doi:10.1007/s40820-019-0255-3.
73. Son BT, Long NV, Nhat Hang NT. The development of biomass-derived carbon-based photocatalysts for the visible-light-driven photodegradation of pollutants: a comprehensive review. RSC Adv. 2021;11(49):30574–96. doi:10.1039/d1ra05079f.
74. Ahmaruzzaman M. Biochar based nanocomposites for photocatalytic degradation of emerging organic pollutants from water and wastewater. Mater Res Bull. 2021;140(27):111262. doi:10.1016/j.materresbull.2021.111262.
75. Liu J, Wang H, Antonietti M. Graphitic carbon nitride "reloaded": emerging applications beyond (photo) catalysis. Chem Soc Rev. 2016;45(8):2308–26. doi:10.1039/c5cs00767d.
76. Thomas A, Fischer A, Goettmann F, Antonietti M, Müller JO, Schlögl R, et al. Graphitic carbon nitride materials: variation of structure and morphology and their use as metal-free catalysts. J Mater Chem. 2008;18(41):4893–908. doi:10.1039/b800274f.
77. Kotbi A, Imran M, Kaja K, Rahaman A, Ressami EM, Lejeune M, et al. Graphene and g-C_3N_4-based gas sensors. J Nanotechnol. 2022;2022:9671619. doi:10.1155/2022/9671619.
78. Yu X, Ng SF, Putri LK, Tan LL, Mohamed AR, Ong WJ. Point-defect engineering: leveraging imperfections in graphitic carbon nitride (g-C(3) N(4)) photocatalysts toward artificial photosynthesis. Small. 2021;17(48):e2006851. doi:10.1002/smll.202006851.
79. Wang X, Maeda K, Thomas A, Takanabe K, Xin G, Carlsson JM, et al. A metal-free polymeric photocatalyst for hydrogen production from water under visible light. Nat Mater. 2009;8(1):76–80. doi:10.1038/nmat2317.
80. Schaber PM, Colson J, Higgins S, Thielen D, Anspach B, Brauer J. Thermal decomposition (pyrolysis) of urea in an open reaction vessel. Thermochim Acta. 2004;424(1–2):131–42. doi:10.1016/j.tca.2004.05.018.
81. Hong Y, Liu E, Shi J, Lin X, Sheng L, Zhang M, et al. A direct one-step synthesis of ultrathin g-C_3N_4 nanosheets from thiourea for boosting solar photocatalytic H_2 evolution. Int J Hydrogen Energy. 2019;44(14):7194–204. doi:10.1016/j.ijhydene.2019.01.274.
82. Huang Y, Lin G, Hua Z, Chen X, Xu X. Effects of thermal program on physicochemical properties and photocatalytic activity of g-C_3N_4 prepared by dicyandiamide pyrolysis. Diam Relat Mater. 2024;141(17):110614. doi:10.1016/j.diamond.2023.110614.

83. Zhang Y, Liu J, Wu G, Chen W. Porous graphitic carbon nitride synthesized via direct polymerization of urea for efficient sunlight-driven photocatalytic hydrogen production. Nanoscale. 2012;4(17):5300–3. doi:10.1039/c2nr30948c.
84. Larsen FK, Hasen Mamakhel A, Overgaard J, Jørgensen JE, Kato K, Brummerstedt Iversen B. Accessing the rich carbon nitride materials chemistry by heat treatments of ammonium thiocyanate, NH_4SCN. Acta Crystallogr B Struct Sci Cryst Eng Mater. 2019;75(Pt 4):621–33. doi:10.1107/S2052520619005791.
85. Peng Q, Dong Y, Li Y. ZnSe semiconductor hollow microspheres. Angew Chem Int Ed. 2003;42(26):3027–30. doi:10.1002/anie.200250695.
86. Li Y, Jin R, Xing Y, Li J, Song S, Liu X, et al. Macroscopic foam-like holey ultrathin g-C_3N_4 nanosheets for drastic improvement of visible-light photocatalytic activity. Adv Energy Mater. 2016;6(24):1601273. doi:10.1002/aenm.201601273.
87. Zhao W, Wang J, Yin R, Li B, Huang X, Zhao L, et al. Single-atom Pt supported on holey ultrathin g-C_3N_4 nanosheets as efficient catalyst for Li-O_2 batteries. J Colloid Interface Sci. 2020;564:28–36. doi:10.1016/j.jcis.2019.12.102.
88. Lu C, Chen X. Nanostructure engineering of graphitic carbon nitride for electrochemical applications. ACS Nano. 2021;15(12):18777–93. doi:10.1021/acsnano.1c06454.
89. Pei J, Li H, Zhuang S, Zhang D, Yu D. Recent advances in g-C_3N_4 photocatalysts: a review of reaction parameters, structure design and exfoliation methods. Catalysts. 2023;13(11):1402. doi:10.3390/catal13111402.
90. Wang L, Wang K, He T, Zhao Y, Song H, Wang H. Graphitic carbon nitride-based photocatalytic materials: preparation strategy and application. ACS Sustainable Chem Eng. 2020;8(43):16048–85. doi:10.1021/acssuschemeng.0c05246.
91. Tibebu S, Worku A, Weldmichael TG. Potential of biochar g-C_3N_4 nanocomposites in soil remediation of 2,4-D with mechanistic insights and future prospects. Discov Environ. 2025;3(1):197. doi:10.1007/s44274-025-00415-3.
92. Li H, Zhang D, Chen Y, Luo W, Xu C, Chen Y, et al. Potassium and phosphorous Co-doped g-C_3N_4/shrimp shell biochar composite attached onto polylactic acid degradable mulching film for photocatalytic removal of atrazine in water and soil. Chem Eng J. 2025;512:162607. doi:10.1016/j.cej.2025.162607.
93. Xi X, Lu Z, Chen HJ, Tian W, Yang YL. Flexible carbon-fiber/g-C_3N_4 nanosheet array as recyclable photocatalysts and photoelectrocatalysts. Sci Rep. 2025;15(1):21090. doi:10.1038/s41598-025-04701-1.
94. Ma R, Sun Y, Zhang H, Zhu J, Tian H, Guo X, et al. Intense interaction between biochar/g-C_3N_4 promotes the photocatalytic performance of heterojunction catalysts. RSC Adv. 2024;14(28):19707–17.
95. Shafique A, Fazal T, Ayub HMU, Abbas Q, Ashraf F. Valorization of algal biomass to synthesize visible-light driven gC_3N_4-biochar composite for dye degradation: tuning of optical-electronic properties and persulfate-photocatalytic mechanistic insights. J Hazard Mater Adv. 2025;18:100683. doi:10.1016/j.hazadv.2025.100683.
96. Liu J, Gao G, Gan L. Metal-free cellulose carbon nanofiber supported graphitic carbon nitride for high-efficient BPA degradation by photcatalytic peroxymonosulfate activation. Catalysts. 2025;15(8):788. doi:10.3390/catal15080788.
97. Mishra PP, Behera D, Suman S, Das N, Tripathy BC, Kumar J, et al. Synergistic efficiency of modified banana leaf derived cellulose-g-C_3N_4 hybrid composite: a sustainable approach for visible-light-driven photodegradation of dyes. RSC Adv. 2025;15(17):13712–27. doi:10.1039/d5ra01156f.
98. Zhong Y, Wang Y, Ji Y, Zhang X, Wang X. Biomass carbon-based composites for adsorption/photocatalysis degradation of VOCs: a comprehensive review. Colloid Interface Sci Commun. 2023;57(15):100749. doi:10.1016/j.colcom.2023.100749.
99. Shi H, Wang W, Mao L, Zhang L, Zhu L, Wu C, et al. Visible light photocatalytic degradation of pesticides and antibiotics by H_3PO_4-activated biochar combined with g-C_3N_4: effects, mechanism, degradation pathway, and toxicity assessment. J Environ Manag. 2025;380(4):124929. doi:10.1016/j.jenvman.2025.124929.
100. Huang F, Tan D, Li D, Guo S, Yan Y, Zhang W. Synthesis of broad spectrum-driven photocatalysts waste biomass-derived carbon quantum dots/g-C_3N_4 with superior energy bands for PPCPs restoration. J Alloys Compd. 2023;947(11):169487. doi:10.1016/j.jallcom.2023.169487.

101. Panwar A, Soni V, Sambyal S, Raizada P, Singh P, Kaya S, et al. Emergence of single atom catalyst and metallic organic frameworks (MOF) derived photocatalytic systems for CO_2 conversion into C1 value added products. J Environ Chem Eng. 2025;13(5):118786. doi:10.1016/j.jece.2025.118786.
102. Zhang Y, Zhao J, Wang H, Xiao B, Zhang W, Zhao X, et al. Single-atom Cu anchored catalysts for photocatalytic renewable H_2 production with a quantum efficiency of 56. Nat Commun. 2022;13(1):58. doi:10.1038/s41467-021-27698-3.
103. Hu Z, Liu W. Conversion of biomasses and copper into catalysts for photocatalytic CO_2 reduction. ACS Appl Mater Interfaces. 2020;12(46):51366–73. doi:10.1021/acsami.0c13323.
104. Li Z, Li K, Ma S, Dang B, Li Y, Fu H, et al. Activation of peroxymonosulfate by iron-biochar composites: comparison of nanoscale Fe with single-atom Fe. J Colloid Interface Sci. 2021;582(Pt B):598–609. doi:10.1016/j.jcis.2020.08.049.
105. Li X, Hu K, Huang Y, Gu Q, Chen Y, Yang B, et al. Upcycling biomass waste into Fe single atom catalysts for pollutant control. J Energy Chem. 2022;69:282–91. doi:10.1016/j.jechem.2022.01.044.
106. Shen M, Hu W, Duan C, Li J, Ding S, Zhang L, et al. Cellulose nanofibers carbon aerogel based single-cobalt-atom catalyst for high-efficiency oxygen reduction and zinc-air battery. J Colloid Interface Sci. 2023;629(Pt A):778–85. doi:10.1016/j.jcis.2022.09.035.
107. Wang Q, Li J, Tu X, Liu H, Shu M, Si R, et al. Single atomically anchored cobalt on carbon quantum dots as efficient photocatalysts for visible light-promoted oxidation reactions. Chem Mater. 2020;32(2):734–43. doi:10.1021/acs.chemmater.9b03708.s001.
108. Zhuang J, Ren S, Zhu B, Han C, Li Y, Zhang X, et al. Lignin-based carbon dots as high-performance support of Pt single atoms for photocatalytic H_2 evolution. Chem Eng J. 2022;446(6):136873. doi:10.1016/j.cej.2022.136873.
109. Gao Z, Meng Y, Koso A, Mishima J, Xie B, Ni Z, et al. Theoretical study on CO_2 reduction to methanol catalyzed by highly stable single-atom transition metal riveted bilayer 2D material. Colloids Surf A Physicochem Eng Aspects. 2022;648:129365. doi:10.1016/j.colsurfa.2022.129365.
110. Hu W, Yang H, Wang C. Progress in photocatalytic CO_2 reduction based on single-atom catalysts. RSC Adv. 2023;13(30):20889–908. doi:10.1039/d3ra03462c.
111. Li D, Zhang F, Luo L, Shang Y, Yang S, Wang J, et al. A universal strategy for green synthesis of biomass-based transition metal single-atom catalysts by simple hydrothermal and compression treatment. Chem Eng J. 2023;461(10):142104. doi:10.1016/j.cej.2023.142104.
112. Cui P, Liu C, Su X, Yang Q, Ge L, Huang M, et al. Atomically dispersed manganese on biochar derived from a hyperaccumulator for photocatalysis in organic pollution remediation. Environ Sci Technol. 2022;56(12):8034–42. doi:10.1021/acs.est.2c00992.
113. Wang D, Deng Y, Liu X, Wang B, Yang F. Recent advances on biomass-derived carbon materials-based electrochemical sensors. Molecules. 2025;30(14):3046. doi:10.3390/molecules30143046.
114. Shyam S, Daimary M, Narayan M, Sarma H. Biochar-based electroanalytical materials: towards sustainable, high-performance electrocatalysts and sensors. Next Mater. 2025;8(19):100873. doi:10.1016/j.nxmate.2025.100873.
115. Chand S, Kumar R, Thakur N, Kumar K, Umar A, Almas T, et al. Sustainable synthesis and multifunctional applications of biowaste-derived carbon nanomaterials and metal oxide composites: a review. Chemosphere. 2025;385:144540. doi:10.1016/j.chemosphere.2025.144540.
116. Zomorodbakhsh S, Dias LD, Calvete MJF, Peixoto AF, Carrilho RMB, Pereira MM. Biochar-based materials for catalytic CO_2 valorization. Catalysts. 2025;15(6):568. doi:10.3390/catal15060568.
117. Chandrasekaran S, Narducci R, Sgreccia E, Haider A, Pasquini L, Marrocchi A, et al. Sustainable electrodes based on biomass-derived catalysts and Ionomers for the Oxygen Reduction Reaction. J Mater Sci Mater Energy. 2025;1(1):7. doi:10.1007/s44308-025-00009-8.
118. Lo M, Tang M, Faye D, Vaiyapuri V, Jayaram A, Mani N, et al. Silver-modified sugarcane bagasse biochar-based electrode materials for the electrochemical detection of mercury ions in aqueous media. Electrochim Acta. 2025;540:147214. doi:10.1016/j.electacta.2025.147214.
119. Ahmed J, Faisal M, Algethami JS, Alkorbi AS, Harraz FA. Facile synthesis of CeO_2·CuO-decorated biomass-derived carbon nanocomposite for sensitive detection of catechol by electrochemical technique. Mater Sci Semicond Process. 2024;172(6):108098. doi:10.1016/j.mssp.2023.108098.

120. Liu X, Zhou Y, Zhou W, Li L, Huang S, Chen S. Biomass-derived nitrogen self-doped porous carbon as effective metal-free catalysts for oxygen reduction reaction. Nanoscale. 2015;7(14):6136–42.
121. Torrarit K, Thipwimonmas Y, Cotchim S, Kongkeaw S, Phonchai A, Limbut W. An electrochemical diclofenac sensor based on an electrode modified with nitrogen-doped biomass-derived carbon and molybdenum trioxide nanoparticles. Talanta. 2026;298(10):128936. doi:10.1016/j.talanta.2025.128936.
122. Jiang W, Zhuo Z, Zhang X, Luo H, He L, Yang Y, et al. Smartphone-based electrochemical sensor for cost-effective, rapid and on site detection of chlorogenic acid in herbs using biomass-derived hierarchically porous carbon synthesized by a soft-hard dual template method. Food Chem. 2024;431(4):137165. doi:10.1016/j.foodchem.2023.137165.
123. Matos R, Marques IS, Fernandes AJS, Peixoto AF, Fernandes DM. Multifunctional N,S-doped biochar decorated with transition metals as electrocatalysts for energy conversion applications. Biomass Bioenergy. 2026;204(2):108463. doi:10.1016/j.biombioe.2025.108463.
124. Zhou Z, Shi Y, Zheng S, Li Z, Xie B, Ji Y, et al. Highly effective porous graphitic carbon derived from bagasse as catalyst for oxygen reduction reaction. Colloids Surf A Physicochem Eng Aspects. 2026;728:138764. doi:10.1016/j.colsurfa.2025.138764.
125. Xu X, Xu R, Zhao Y, Wu Y, Yuan Q, Sun K, et al. Boron-doped biomass carbon nanostructures as electrocatalysts for the two-electron oxygen reduction reaction. ACS Appl Nano Mater. 2024;7(16):18912–9. doi:10.1021/acsanm.4c02704.
126. Sirichandana B, Silviya R, Bhat SV, Patel N, Hegde G. Biomass-derived carbon supported cobalt-phospho-boride as a bifunctional electrocatalyst for enhanced alkaline water splitting. Nanoscale Adv. 2025;7(13):4056–66. doi:10.1039/d5na00213c/v2/response1.
127. Kumar S, Anshu A, Kumar R, Anantharamaiah PN, Yadav A, Patil PN, et al. Cobalt nanoparticles embedded in N-doped carbon nanostructure sourced from banana leaves for oxygen and hydrogen generation. Energy Fuels. 2025;39(44):21498–510. doi:10.1021/acs.energyfuels.5c04282.
128. Malode SJ, Shanbhag MM, Kumari R, Dkhar DS, Chandra P, Shetti NP. Biomass-derived carbon nanomaterials for sensor applications. J Pharm Biomed Anal. 2023;222:115102. doi:10.1016/j.jpba.2022.115102.
129. Xiao X, Li L, Deng H, Zhong Y, Deng W, Xu Y, et al. Biomass-derived 2D carbon materials: structure, fabrication, and application in electrochemical sensors. J Mater Chem B. 2023;11(45):10793–821. doi:10.1039/d3tb01910a.
130. Onfray C, Thiam A. Biomass-derived carbon-based electrodes for electrochemical sensing: a review. Micromachines. 2023;14(9):1688. doi:10.3390/mi14091688.
131. El-Sayed SA. Chemical products yielded from different pyrolysis processes of rice waste residues: a comprehensive review. Biomass Convers Biorefin. 2025;15(14):20615–55. doi:10.1007/s13399-025-06624-3.
132. Duan Y, Lv T, Dong K, Zheng F, Li X, Qi Y, et al. A novel hydrogel electrolyte for all-climate high-performance flexible zinc-ion hybrid capacitors within temperature range from −50°C to 100°C. Chem Eng J. 2023;474(23):145551. doi:10.1016/j.cej.2023.145551.
133. Wen T, Li R, Xu P, Liu X, Wang P, Lei X, et al. Scalable synthesis of $Ta_{1.1}O_{1.05}$/biomass carbon composite with multiple structure engineering by boron-doped graphene quantum dot for high-energy supercapacitor. Appl Surf Sci. 2023;615(30):156387. doi:10.1016/j.apsusc.2023.156387.
134. Guo Y, Wang L, Zhang L, Song Y, Liu W, Li C, et al. Diminishing coking in steam reforming of acetic acid through modification of reaction intermediates via adding carbonates to Ni/biochar catalyst. Appl Catal A Gen. 2026;709(6):120645. doi:10.1016/j.apcata.2025.120645.
135. Huang ST, Lei YQ, Guo PR, Chen HX, Gan SC, Diao ZH. Electrocatalytic degradation of Favipiravir by heteroatom (P and S) doped biomass-derived carbon with high oxygen reduction reaction activity. Chem Eng J. 2024;484(48):149543. doi:10.1016/j.cej.2024.149543.
136. Li M, Zhou Y, Lin L, Li W. Legume root nodule derived porous carbon materials through the *in situ* ZIF-8 activation strategy. RSC Adv. 2025;15(21):16267–75. doi:10.1039/d5ra01675d.
137. Zhang X, Wang X, Yao D, Guo M, Lv J, Vongsvivut JP, et al. Porous N, O, S-doped carbon from feathers drives pH-universal H_2O_2Electroproduction. Adv Funct Mater. 2026;36(17):e24856. doi:10.1002/adfm.202524856.

138. Balasubramanian D, Varadharajan H, Venugopal IP. Biomass-derived porous carbon from banana leaves for efficient supercapacitor applications–An experimental analysis. Biomass Bioenergy. 2025;201(Part 2):108104. doi:10.1016/j.biombioe.2025.108104.
139. Simon S, Cherian AR, Sreeja PB. Transforming invasive weeds into energy solutions: water hyacinth-based hybrid electrodes for green supercapacitors. RSC Adv. 2025;15(22):17302–16. doi:10.1039/d5ra02140e.
140. Bai X, Wang Z, Luo J, Wu W, Liang Y, Tong X, et al. Hierarchical porous carbon with interconnected ordered pores from biowaste for high-performance supercapacitor electrodes. Nanoscale Res Lett. 2020;15(1):88. doi:10.1186/s11671-020-03305-0.
141. Wassner M, Eckardt M, Reyer A, Diemant T, Elsaesser MS, Behm RJ, et al. Synthesis of amorphous and graphitized porous nitrogen-doped carbon spheres as oxygen reduction reaction catalysts. Beilstein J Nanotechnol. 2020;11:1–15. doi:10.3762/bjnano.11.1.
142. Zha Z, Zhang Z, Xiang P, Zhu H, Zhou B, Sun Z, et al. One-step preparation of eggplant-derived hierarchical porous graphitic biochar as efficient oxygen reduction catalyst in microbial fuel cells. RSC Adv. 2021;11(2):1077–85. doi:10.1039/d0ra09976g.
143. Cosenza A, Roiron C, Ferro G, Atanassov P. Nitrogen-doped carbon supports for Pt-based fuel cell electrocatalysts. Chem Eng J. 2025;512(28):162816. doi:10.1016/j.cej.2025.162816.
144. Yun WC, Yang J, Lee D, Lee J, Kim J, Byeon A, et al. Enhanced electroproduction of hydrogen peroxide with oxidized boron-doped carbon catalysts synthesized from gaseous CO_2. J CO_2 Util. 2024;84:102833. doi:10.1016/j.jcou.2024.102833.
145. Choi JW, Byeon A, Kim S, Hwang CK, Zhang W, Lee J, et al. Mesoporous boron-doped carbon with curved B_4C active sites for highly efficient H_2O_2 electrosynthesis in neutral media and air-supplied environments. Adv Mater. 2025;37(9):e2415712. doi:10.1002/adma.202415712.
146. Qu S, Cao Y, Zhang J, Ma P, Liang Z, Cao R. Sulfur-doped cobalt–nitrogen–carbon materials for efficient oxygen electrocatalysis. Sustainable Energy Fuels. 2026;10(1):285–93. doi:10.1039/d5se01222h.
147. Peng Z, Chen D, Nie J, Jia Z, Guo J, Jadhav CD, et al. Derived S/N/Co Co-doped porous carbon as superior oxygen reduction reaction catalysts. Diam Relat Mater. 2025;153:112058. doi:10.1016/j.diamond.2025.112058.
148. Tang Y, Zeng Z, Yi L, Zhu S, Li X, Li H, et al. Heteroatom-anchored porous carbon as efficient electrocatalyst for oxygen reduction reaction. Energy Fuels. 2022;36(4):2068–74. doi:10.1021/acs.energyfuels.1c04371.
149. Kaare K, Volperts A, Plavniece A, Walke P, Käämbre T, Noor N, et al. Heteroatom-doped carbon nanomaterials derived from black liquor for electrochemical oxygen reduction reaction. ACS Sustainable Resour Manage. 2024;1(8):1705–16. doi:10.1021/acssusresmgt.4c00022.
150. Qi P, Wang J, Djitcheu X, He D, Liu H, Zhang Q. Techniques for the characterization of single atom catalysts. RSC Adv. 2022;12(2):1216–27. doi:10.1039/d1ra07799f.
151. Egerton RF, Watanabe M. Characterization of single-atom catalysts by EELS and EDX spectroscopy. Ultramicroscopy. 2018;193(3):111–7. doi:10.1016/j.ultramic.2018.06.013.
152. Li Z, Yang H, Cheng W, Tian L. Recent progress of *in situ*/operando characterization techniques for electrocatalytic energy conversion reaction. Chin Chem Lett. 2024;35(9):109237. doi:10.1016/j.cclet.2023.109237.
153. Meyer JC, Eder F, Kurasch S, Skakalova V, Kotakoski J, Park HJ, et al. Accurate measurement of electron beam induced displacement cross sections for single-layer graphene. Phys Rev Lett. 2012;108(19):196102. doi:10.1103/PhysRevLett.108.196102.
154. Linck M, Hartel P, Uhlemann S, Kahl F, Müller H, Zach J, et al. Chromatic aberration correction for atomic resolution TEM imaging from 20 to 80 kV. Phys Rev Lett. 2016;117(7):076101. doi:10.1103/PhysRevLett.117.076101.
155. Centeno TA, Stoeckli F. The assessment of surface areas in porous carbons by two model-independent techniques, the DR equation and DFT. Carbon. 2010;48(9):2478–86. doi:10.1016/j.carbon.2010.03.020.